



# Air-Stable $\text{Na}_x\text{TMO}_2$ Cathodes for Sodium Storage

Yi Zhang, Renyuan Zhang\* and Yunhui Huang

Institute of New Energy for Vehicles, School of Materials Science and Engineering, Tongji University, Shanghai, China

Sodium-ion batteries are considered to be the most promising alternative to lithium-ion batteries for large-scale stationary energy storage applications due to the abundant sodium resource in the Earth's crust and as a result, relatively low cost. Sodium layered transition metal oxides ( $\text{Na}_x\text{TMO}_2$ ) are proper Na-ion cathode materials because of low cost and high theoretical capacity. Currently most researchers focus on the improvement of electrochemical performance such as high rate capability and long cycling stability. However, for  $\text{Na}_x\text{TMO}_2$ , the structure stability against humid atmosphere is essentially important since most of them are instable in air, which is not favorable for practical application. Here we provide a comprehensive review of recent progresses on air-stable  $\text{Na}_x\text{TMO}_2$  oxides. Several effective strategies are discussed, and further investigations on the air-stable cathodes are prospected.

**Keywords:** layered transition metal oxides, air-stable, cathode, sodium-ion battery, water insertion, H ion exchange

## OPEN ACCESS

### Edited by:

Fan Zhang,  
Fudan University, China

### Reviewed by:

Juchen Guo,  
University of California, Riverside,  
United States  
Jianping Yang,  
Donghua University, China

### \*Correspondence:

Renyuan Zhang  
ryzhang@tongji.edu.cn

### Specialty section:

This article was submitted to  
Nanoscience,  
a section of the journal  
Frontiers in Chemistry

Received: 17 February 2019

Accepted: 25 April 2019

Published: 14 May 2019

### Citation:

Zhang Y, Zhang R and Huang Y (2019)  
Air-Stable  $\text{Na}_x\text{TMO}_2$  Cathodes for  
Sodium Storage. *Front. Chem.* 7:335.  
doi: 10.3389/fchem.2019.00335

## INTRODUCTION

The growing demand for large-scale energy storage applications has driven the research interest into new energy storage systems with low cost. Although lithium-ion battery (LIB) can deliver high energy and power density, the limited resource and the rising cost of lithium may restrict their application in grid scale energy storage. Recently, sodium-ion battery (SIB), which owns a similar chemical storage mechanism to LIB, has been rapidly developed as a complementary technology. As the second lightest alkali metal, sodium resource is inexpensive and almost globally available. The common abundant sodium salt such as  $\text{Na}_2\text{SO}_4$ ,  $\text{NaCl}$ , and  $\text{Na}_2\text{CO}_3$  could be obtained from marine or mineral. In addition, copper foil can be replaced by cheaper aluminum foil for anode current collector since sodium has no reaction with aluminum. Therefore, SIB has received considerable attention as a promising alternative to LIB (Dunn et al., 2011; Yang et al., 2011, 2017; Palomares et al., 2013; Pan et al., 2013; Yabuuchi et al., 2014; Han et al., 2015; Kubota and Komaba, 2015; Kundu et al., 2015; Xiang et al., 2015; Hwang et al., 2017; Luo et al., 2017; Nayak et al., 2018; Zhu et al., 2019).

The SIB system consists of five parts: cathode, anode, membrane, electrolyte and current collector, which has the same structure as LIB. **Figure 1** shows typical configuration of a SIB coin cell, in which sodium layered transition metal oxide ( $\text{Na}_x\text{TMO}_2$ ) and hard carbon are employed as cathode and anode, respectively. During the charge process, the  $\text{Na}^+$  and  $e^-$  migrates to hard carbon anode with voltage increasing. During the discharge process,  $\text{Na}^+$  and  $e^-$  return to  $\text{Na}_x\text{TMO}_2$  cathode reversibly with voltage decreasing. The overall reaction can be described as:



Numerous cathode materials such as polyanion compounds (Tripathi et al., 2013; Zhang Y. et al., 2016), layered transition metal (TM) oxides (Roger et al., 2007; Berthelot et al., 2011; Carlier et al., 2011) and Prussian blue or Metal-Organic compounds (Fang et al., 2017; Su et al., 2017;

Qian et al., 2018) have been applied as  $\text{Na}^+$  host materials. Layered TM oxides show a high theoretical capacity among these cathode materials (Wang et al., 2018c). In addition, taking the preparation process and cost into consideration, the layered transition metal oxides are the optimal choice for practical application because they can be easily obtained by calcining the precursors in air. As a result, the layered transition metal oxides with general formula  $\text{Na}_x\text{TMO}_2$  have attracted more and more attention since the first report by Delmas' group in the 1980s (Delmas et al., 1980, 1981).

Most of researches about  $\text{Na}_x\text{TMO}_2$  focused on the improvement of electrochemical properties, such as: (i) eliminating  $\text{Na}^+$  vacancy ordering to improve rate capability; (Wang et al., 2015, 2018a; Kang et al., 2018) (ii) suppressing phase transition or surface coating to achieve long cycling life; (Wang et al., 2016c; Wang P.-F. et al., 2017; You et al., 2017; Sathiyaraj et al., 2018) (iii) exploring oxygen ion redox mechanism

to achieve high energy density (Rozier et al., 2015; Kim et al., 2017; Bai et al., 2018; Maitra et al., 2018; Qiao et al., 2018; Rong et al., 2018), and so on. However, most  $\text{Na}_x\text{TMO}_2$  materials are hygroscopic and air-instable, which limit their practical applications because huge cost will be spent on materials' storage and transportation (Blesa et al., 1993; Franger et al., 2000; Lu and Dahn, 2001b; Caballero et al., 2002; Monyoncho and Bissessur, 2013; Duffort et al., 2015; Kubota and Komaba, 2015; Boyd et al., 2018; You et al., 2018). So in recent years, the design and synthesis of air-stable  $\text{Na}_x\text{TMO}_2$  materials have become a hot topic. In this review, we summarize the recent progress on air-stable  $\text{Na}_x\text{TMO}_2$  materials from structure understanding to corresponding solutions, and at the same time we address the remaining problems and challenges for further development.

## STRUCTURE OF $\text{Na}_x\text{TMO}_2$

In  $\text{Na}_x\text{TMO}_2$  compounds, TM layers are usually occupied by Ti, (Senguttuvan et al., 2011; Wu D. et al., 2015) V, (Hamani et al., 2011; Guignard et al., 2013; Wang et al., 2018d) Cr, (Braconnier et al., 1982; Yu et al., 2015) Mn, (Ma et al., 2011) Fe, (Blesa et al., 1993; Yabuuchi et al., 2012b) Co, (Berthelot et al., 2011; Rai et al., 2014) Ni, (Vassilaras et al., 2013; Wang et al., 2018b) Cu, (Ono et al., 2014; Jiang et al., 2018; Ono, 2018) a mixture of two (Saadouni et al., 1996; Yabuuchi et al., 2012a; Mortemard de Boisse et al., 2013; Gonzalo et al., 2014; Guo et al., 2014; Kalluri et al., 2014; Zhu et al., 2014, 2016; Chen et al., 2015; Jiang et al., 2015; Kang et al., 2015; Wang et al., 2015, 2016d; Bucher et al., 2016; Kee et al., 2016; Liu et al., 2016; Manikandan et al., 2017; Sabi et al., 2017; Song et al., 2017) or more elements (Lu and Dahn, 2001b; Buchholz et al., 2014; Li et al., 2014; Liu et al., 2015; Li Y. et al., 2015; Li Z.-Y. et al., 2015; Yue et al., 2015; Han et al., 2016a; Kang et al., 2016; Qi et al., 2016; Satyanarayana et al., 2016; Sun et al., 2016; Wang et al., 2016b; Zhang X.-H. et al., 2016; Wang L. et al., 2017; Zheng and Obrovac, 2017) The corresponding

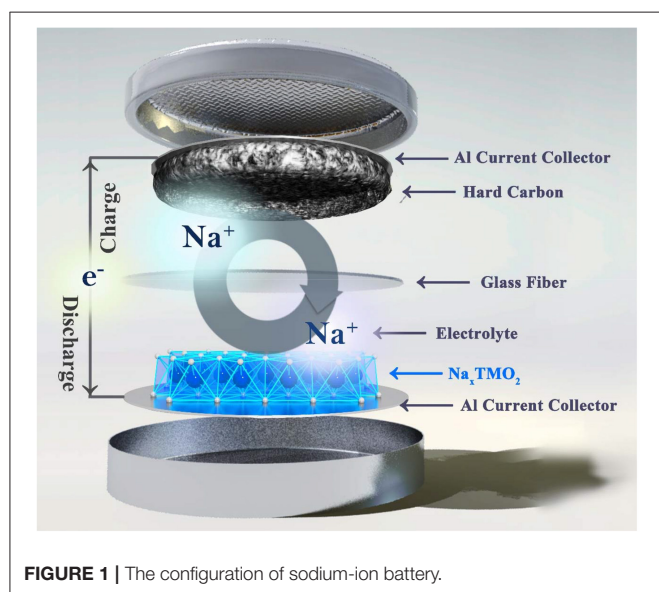


FIGURE 1 | The configuration of sodium-ion battery.

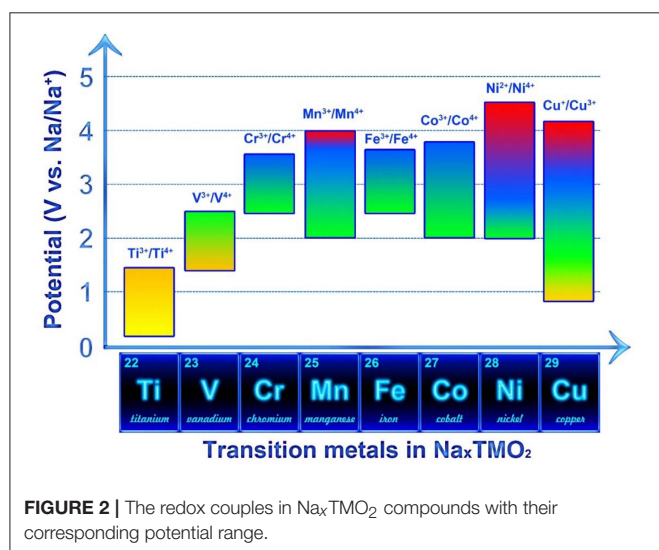


FIGURE 2 | The redox couples in  $\text{Na}_x\text{TMO}_2$  compounds with their corresponding potential range.

TABLE 1 | Ionic radius of metal ions.

Metal ion	Coordination number	Ionic radius (Å)
$\text{Li}^+$	VI	0.76
$\text{Mg}^{2+}$	VI	0.72
$\text{Al}^{3+}$	VI	0.535
$\text{Ti}^{4+}$	VI	0.605
$\text{V}^{5+}$	VI	0.54
$\text{Cr}^{3+}$	VI	0.615
$\text{Mn}^{4+}$	VI	0.53
$\text{Fe}^{3+}$	VI	0.55(L); 0.645(H)*
$\text{Co}^{3+}$	VI	0.545(L); 0.61 (H)
$\text{Ni}^{2+}$	VI	0.69
$\text{Cu}^{2+}$	VI	0.73
$\text{Zn}^{2+}$	VI	0.74

\*L means low spin while H means high spin.

redox potential ranges of these TM are presented in **Figure 2**.  $\text{Na}_x\text{TiO}_2$  compound is usually used as anode material due to its low redox potential range.  $\text{Na}_x(\text{Ni}_y\text{Mn}_{1-y})\text{O}_2$  compound has been thoroughly investigated as cathode material because of the relatively high redox potential and theoretical capacity. (Lu and Dahn, 2001a; Fielden and Obrovac, 2015) V, Cr and Co substitution also shows a proper potential range for cathode but it may not be suitable for practical application since V, Cr, and Co are expensive and toxic. Although Fe and Cu are almost electrochemically inactive when used as  $\text{LiTMO}_2$  for LIB system, (Ado et al., 1997; Arachi et al., 2012) these two elements are proven to be highly active in  $\text{Na}_x\text{TMO}_2$  as Na-ion host. (Yabuuchi et al., 2012a; Ono, 2018) Since Ni and Co resources are mostly consumed by LIB system, the abundant Fe and Cu resources with low price are suitable for  $\text{Na}_x\text{TMO}_2$  as sodium storage materials. (Li Y. et al., 2015; Mu et al., 2015) In addition, electrochemically inactive metal ions such as  $\text{Li}^+$ ,  $\text{Mg}^{2+}$  and  $\text{Zn}^{2+}$  could also be introduced into the TM layer for the improvement of electrochemical performance (Xu et al., 2014; Wu X. et al., 2015; Wang et al., 2016c). **Table 1** lists the most common metal ions for the construction of TM layers and their corresponding ionic radii with coordination number

of six (Shannon, 1976). Cations with similar ionic radius can partially substitute each other to form solid solutions, and hence various  $\text{Na}_x\text{TMO}_2$  compounds could be designed by choosing two or more proper metal ions for the TM layer to improve electrochemical performance.

The crystal structure of  $\text{Na}_x\text{TMO}_2$  can be usually classified into two types, P2 and O3 (**Figure 3**). The symbols of “P” and “O” are from the abbreviation of “prismatic” and “octahedral,” “2” and “3” represents the stacking arrangement per unit of O ions. For P2 type structure (usually  $x = 2/3$ ), Na ions occupy two different prismatic sites, one shares faces between  $\text{TMO}_6$  octahedra called  $\text{Na}_f$  sites and another shares edges between  $\text{TMO}_6$  octahedra called  $\text{Na}_e$  sites. TM ions are surrounded by oxygen frameworks with a stacking mode of ABBA. For O3 structure (usually  $x = 1$ ), all Na ions share one edge and one face with  $\text{TMO}_6$  octahedra. The oxygen frameworks are arranged in ABCABC pattern (Delmas et al., 1980, 1981; Shu and Chou, 2008; Morris et al., 2009; Toumar et al., 2015; Zheng C. et al., 2017).

### Influence of Air on $\text{Na}_x\text{TMO}_2$

So far, many researches have proven that the water and  $\text{CO}_2$  molecules from air can react with  $\text{Na}_x\text{TMO}_2$ , bringing

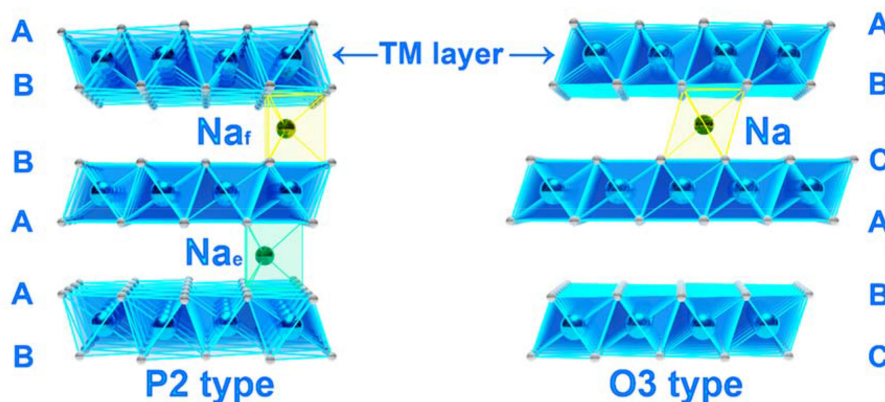


**FIGURE 3** | The schematic of the crystal structure for layered sodium TM oxides, left is P2 type and right is O3 type.

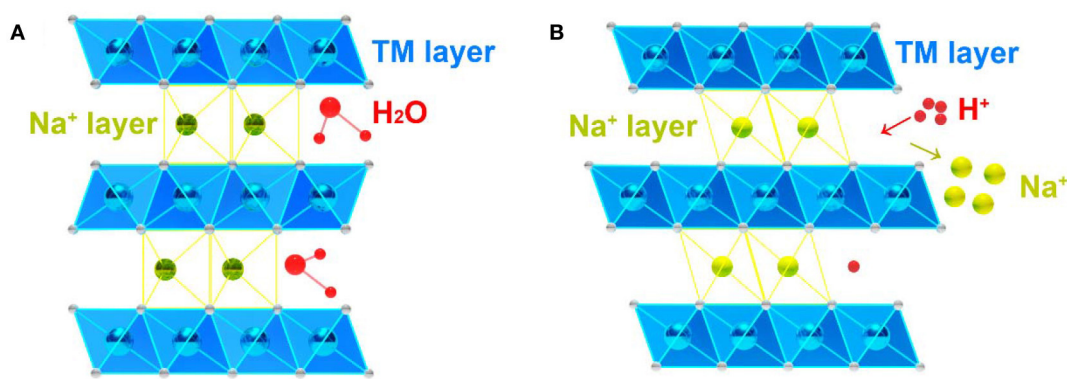


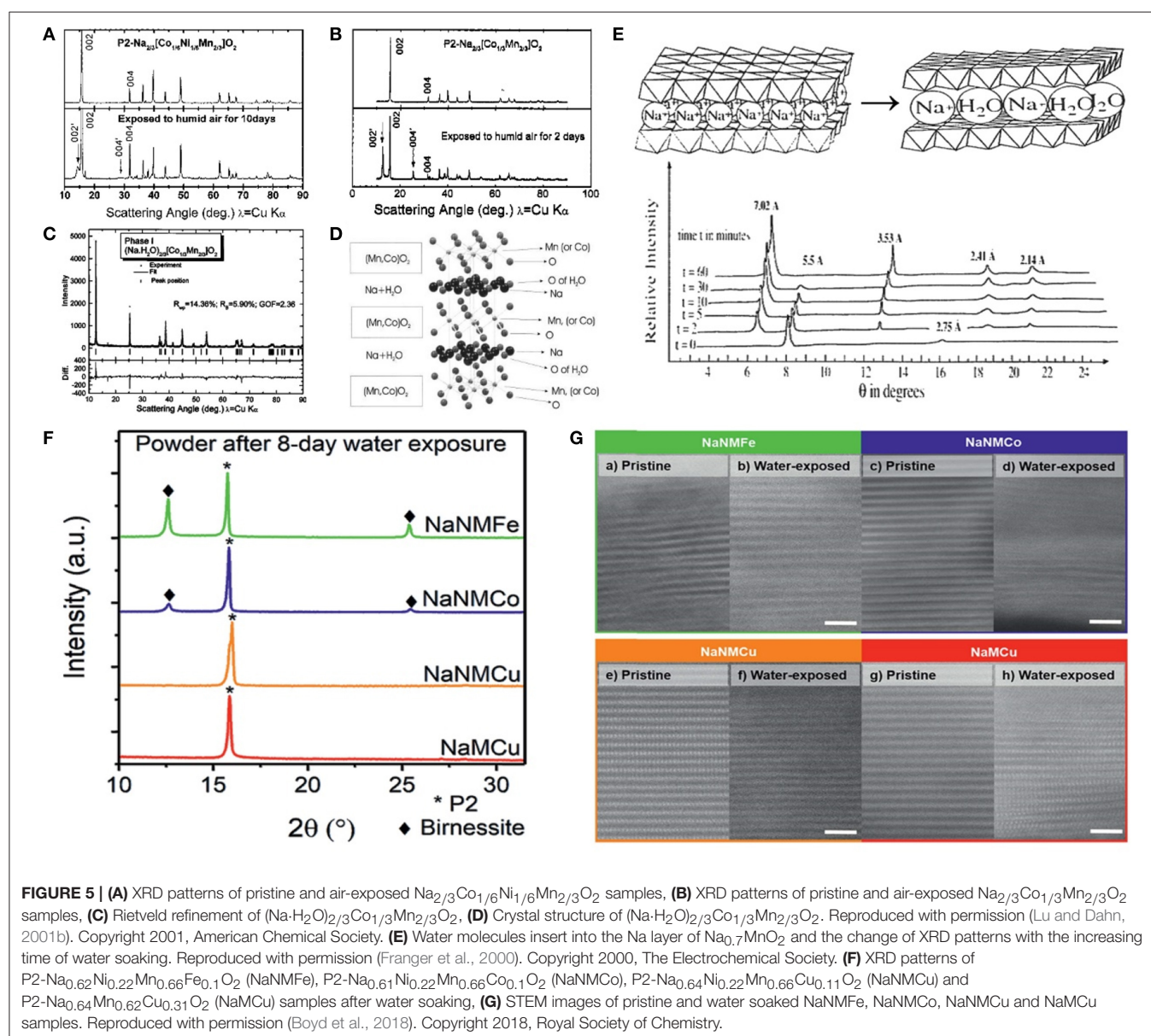
**FIGURE 4** | (A) Insertion of water molecules in  $\text{Na}^+$  layer, (B) Ion exchange between  $\text{H}^+$  and  $\text{Na}^+$  in  $\text{Na}^+$  layer.

negative influence on its morphology, crystal structure and electrochemical performance. The water molecules are easy to react with air-instable  $\text{Na}_x\text{TMO}_2$  by inserting into the Na layer (Le Goff et al., 1993; Paulsen and Dahn, 1999; Franger et al., 2000; Lu and Dahn, 2001b; Caballero et al., 2002; Duffort et al., 2015; Boyd et al., 2018) or exchanging  $\text{Na}^+$  with  $\text{H}^+$ , (Blesa et al., 1993; Monyoncho and Bissessur, 2013; Kubota and Komaba, 2015; Han et al., 2016b; Yao et al., 2017) leading to the expansion of interlayer spacing and the formation of impure phase (Figure 4). While  $\text{CO}_2$  can transform to  $\text{CO}_3^{2-}$  on the surface of  $\text{Na}_x\text{TMO}_2$  (Duffort et al., 2015; You et al., 2018). These air exposed  $\text{Na}_x\text{TMO}_2$  usually show serious capacity decay and large polarization because of: (i) the side reaction between water and electrolyte (Kawamura et al., 2006; Lux et al., 2012; Han et al., 2016b); (ii) the

active-materials' surface dissolution triggered by the acid attack of proton, which is released by water molecules (Blyr et al., 1998; Thackeray et al., 1998; Benedek and van de Walle, 2008); (iii) capacity and electronic conductivity decrease caused by inactive  $\text{Na}_2\text{CO}_3$  layer (Duffort et al., 2015; You et al., 2018). Therefore, the air-instable  $\text{Na}_x\text{TMO}_2$  cannot maintain its original crystal structure and electrochemical property under moisture atmosphere condition.

## Reaction Mechanisms of Water on $\text{Na}_x\text{TMO}_2$

Water molecules can insert into Na layer to form a  $\text{Na}_x\text{TMO}_2 \cdot y\text{H}_2\text{O}$  hydrate phase, which usually occurs in P2 type structure (Le Goff et al., 1993; Franger et al., 2000; Lu and Dahn, 2001b; Caballero et al., 2002; Duffort et al.,



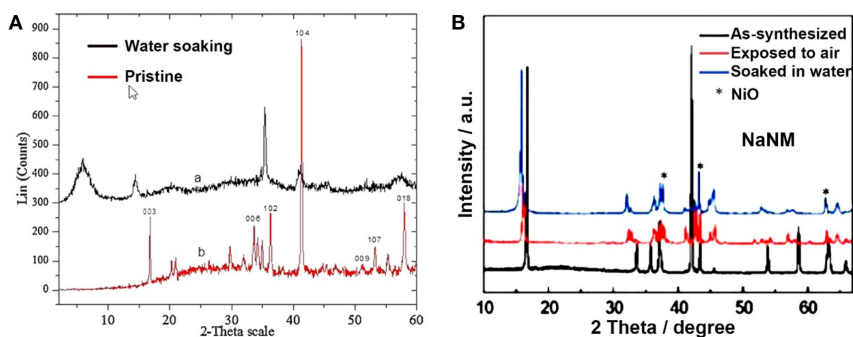


**FIGURE 6 | (A)** XRD patterns of pristine and water soaked NaFeO<sub>2</sub> samples. Reproduced with permission (Monyoncho and Bissessur, 2013). Copyright 2013, Elsevier. **(B)** XRD patterns of pristine, air exposed and water soaked NaNi<sub>0.5</sub>Mn<sub>0.5</sub>O<sub>2</sub> samples. Reproduced with permission (Yao et al., 2017). Copyright 2017, American Chemical Society.

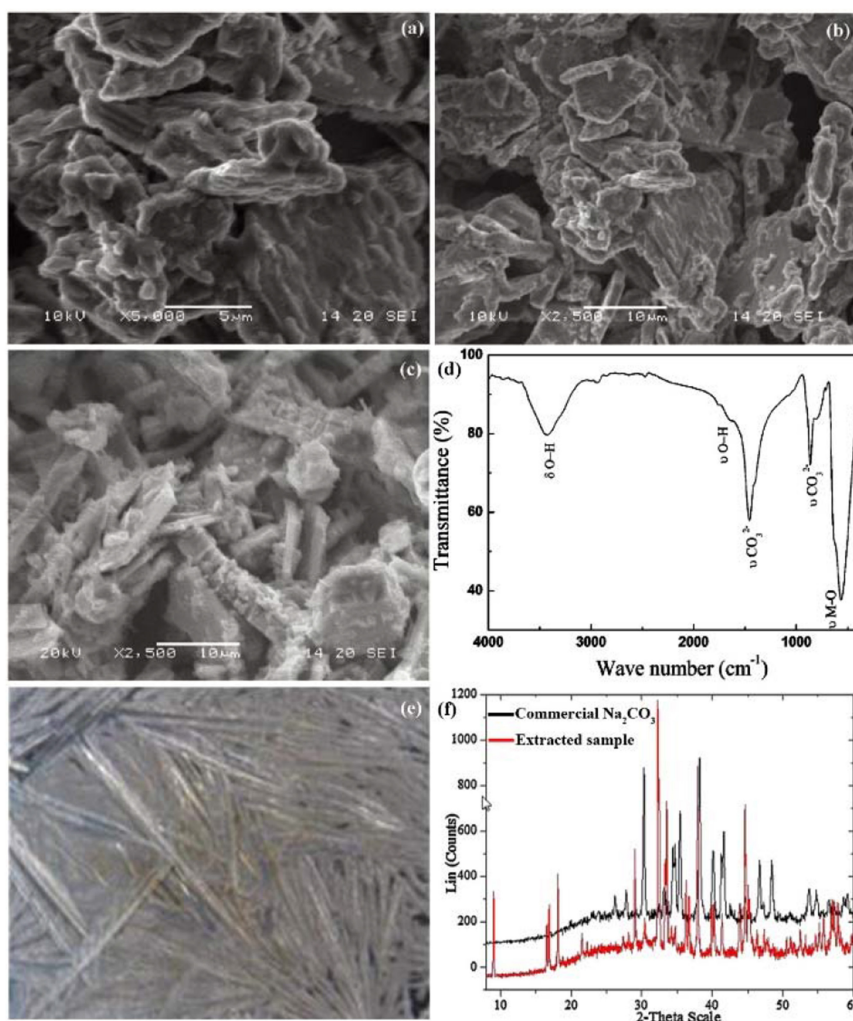
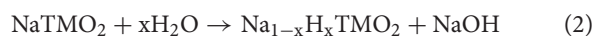


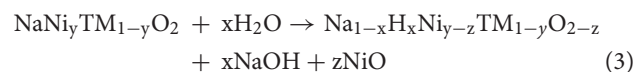
**FIGURE 7 | (a)** SEM images of (a) pristine NaNi<sub>1/3</sub>Mn<sub>1/3</sub>Co<sub>1/3</sub>O<sub>2</sub>, (b) NaNi<sub>1/3</sub>Mn<sub>1/3</sub>Co<sub>1/3</sub>O<sub>2</sub> after 15 days air-exposure, (c) NaNi<sub>1/3</sub>Mn<sub>1/3</sub>Co<sub>1/3</sub>O<sub>2</sub> after 30 days air-exposure. (d) Infrared spectrum of NaNi<sub>1/3</sub>Mn<sub>1/3</sub>Co<sub>1/3</sub>O<sub>2</sub> after 30 days air-exposure. Reproduced with permission (Sathiya et al., 2012). Copyright 2012, American Chemical Society. (e) SEM image of extracted sample, the sample is prepared by drying the aqueous solution of water-NaFeO<sub>2</sub> mixture, (f) XRD patterns of the extracted sample and commercial Na<sub>2</sub>CO<sub>3</sub>. Reproduced with permission (Monyoncho and Bissessur, 2013). Copyright 2013, Elsevier.

2015; Boyd et al., 2018). In 2001, Lu et al. (Lu and Dahn, 2001b) studied the water insertion reaction mechanism for the first time in  $P2\text{-Na}_{2/3}\text{Co}_x\text{Ni}_{1/3-x}\text{Mn}_{2/3}\text{O}_2$  compound ( $x = 1/6$  or  $1/3$ ). Compared with the XRD patterns of pristine  $\text{Na}_{2/3}\text{Co}_x\text{Ni}_{1/3-x}\text{Mn}_{2/3}\text{O}_2$ , two new peaks around  $14^\circ$  and  $28^\circ$  were observed after exposing  $\text{Na}_{2/3}\text{Co}_x\text{Ni}_{1/3-x}\text{Mn}_{2/3}\text{O}_2$  samples in humid air environment (Figures 5A,B). These two peaks were assigned as hydrate phase due to the insertion of water molecules in Na layers. Rietveld refinement of hydrate  $\text{Na}_{2/3}\text{Co}_{1/3}\text{Mn}_{2/3}\text{O}_2 \cdot y\text{H}_2\text{O}$  indicated that the ratio of water/Na is close to 1:1 and the oxygen atoms from water was in the 2c site of the crystal structure (Figures 5C,D). Franger et al. (Franger et al., 2000) investigated the influence of water soaking on  $\alpha\text{-Na}_{0.7}\text{MnO}_2$ . With the increasing of water soaking time, the two peaks around  $8^\circ$  and  $16^\circ$  were vanished and four new peaks around  $6.5^\circ$ ,  $13^\circ$ ,  $19^\circ$  and  $21^\circ$  appeared gradually. The  $\alpha\text{-Na}_{0.7}\text{MnO}_2$  was totally transformed to  $\text{Na}_{0.45}\text{MnO}_2 \cdot 0.6\text{H}_2\text{O}$  after 60 min of water soaking treatment (Figure 5E). In 2018, Boyd et al. compared the air-stability of  $P2\text{-Na}_{0.62}\text{Ni}_{0.22}\text{Mn}_{0.66}\text{Fe}_{0.1}\text{O}_2$  (NaNMFe),  $P2\text{-Na}_{0.61}\text{Ni}_{0.22}\text{Mn}_{0.66}\text{Co}_{0.1}\text{O}_2$  (NaNMCo),  $P2\text{-Na}_{0.64}\text{Ni}_{0.22}\text{Mn}_{0.66}\text{Cu}_{0.11}\text{O}_2$  (NaNMCu) and  $P2\text{-Na}_{0.64}\text{Mn}_{0.62}\text{Cu}_{0.31}\text{O}_2$  (NaMCu) samples. After air-exposure treatment of these four samples for 8 days, the XRD patterns of NaNMCu and NaMCu samples remained unchanged, while two new peaks around  $12.5^\circ$  and  $25^\circ$  appeared in the patterns of NaNMFe and NaNMCo samples, indicating that water can insert in the interlayer spacing of NaNMFe and NaNMCo samples (Figure 5F). From the STEM images of these four samples before and after air-exposure, an obvious extension in interlayer spacing could be seen after air-exposure, proving the insertion of water molecules in the interlayer spacing (Figure 5G). Although water molecules can insert into the interlayer spacing of  $P2\text{-Na}_x\text{TMO}_2$  to form a  $P2\text{-Na}_x\text{TMO}_2 \cdot y\text{H}_2\text{O}$  hydrate phase,  $\text{Na}_x\text{TMO}_2$  phase can be regenerated by heat treatment at  $200^\circ\text{C}$  to remove the water molecules (Lu and Dahn, 2001b).

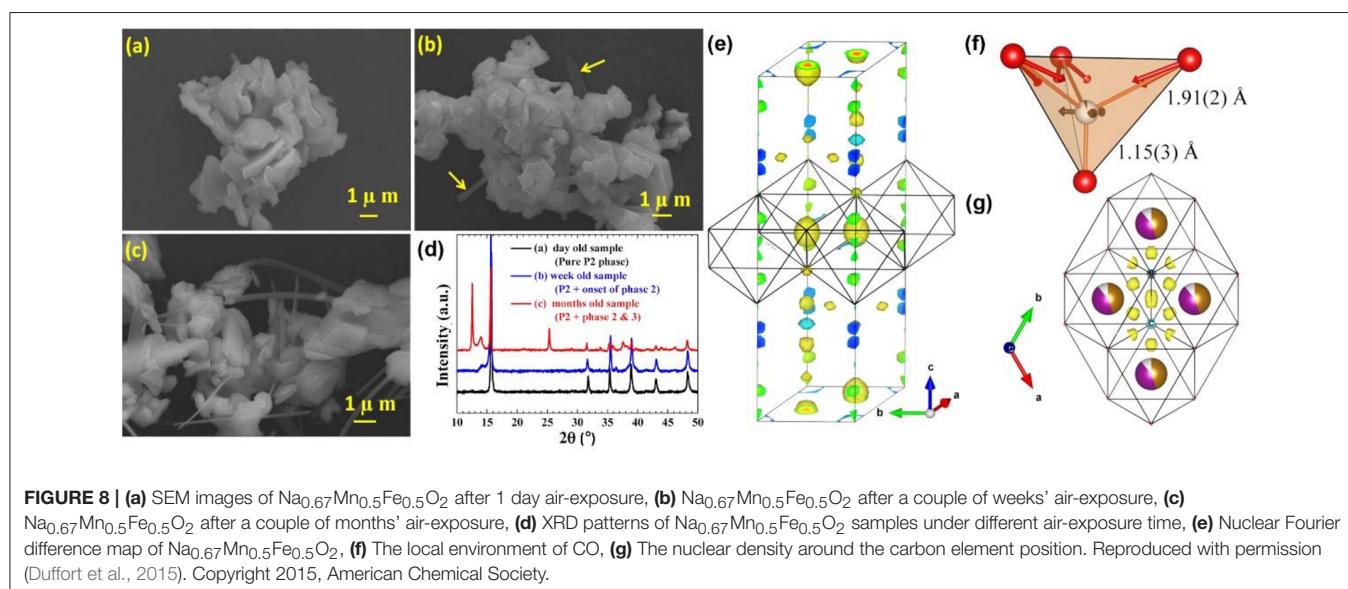
For most O3-type  $\text{NaTMO}_2$ , water molecules can release  $\text{H}^+$  to exchange the  $\text{Na}^+$ , (Blesa et al., 1993; Monyoncho and Bissessur, 2013; Kubota and Komaba, 2015; Han et al., 2016b; Yao et al., 2017) which could be regarded as hydrolysis reaction:



Specially, if the TM layers contain a certain amount of  $\text{Ni}^{2+}$  ions, NiO would be emerged during the air exposure treatment:



This hydrolysis phenomenon has been confirmed in  $\text{NaNi}_{0.5}\text{Mn}_{0.5}\text{O}_2$ ,  $\text{NaNi}_{0.7}\text{Mn}_{0.15}\text{Co}_{0.15}\text{O}_2$  and  $\text{NaFeO}_2$  compounds (Blesa et al., 1993; Monyoncho and Bissessur, 2013; Kubota and Komaba, 2015; You et al., 2018). A simple way to verify this hydrolysis reaction is to analyze the change of pH value after soaking  $\text{NaTMO}_2$  in deionized water due to the release of NaOH (Blesa et al., 1993). In 2013, Monyoncho and Bissessur reported that the pH of aqueous solution was higher than 12 after mixing O3- $\text{NaFeO}_2$  sample with deionized water (Monyoncho and Bissessur, 2013). In addition, compared with the XRD patterns of pristine  $\text{NaFeO}_2$  sample, the 003 peak of hydrolysis  $\text{Na}_{1-x}\text{H}_x\text{FeO}_2$  sample became broader and shifted to low angle (Figure 6A), indicating the formation of a disordered crystal structure. Wang et al. investigated the hydrolysis reaction of O3- $\text{NaNi}_{0.5}\text{Mn}_{0.5}\text{O}_2$  sample by testing the temperature after water soaking because this reaction can release heats (Yao et al., 2017). After  $\text{NaNi}_{0.5}\text{Mn}_{0.5}\text{O}_2$  was added into water, the temperature of the water was increased from  $24.4$  to  $30.8^\circ\text{C}$ . In contrast to the XRD pattern of as-synthesized sample, the 003 and 006 peaks of water soaked  $\text{NaNi}_{0.5}\text{Mn}_{0.5}\text{O}_2$  shifted to low angle with the generation of NiO impurity phase (Figure 6B). Importantly, unlike P2 type, the hydrolysis reaction between O3 type  $\text{NaTMO}_2$  and water is irreversible.



## Reaction Mechanisms of CO<sub>2</sub> on Na<sub>x</sub>TMO<sub>2</sub>

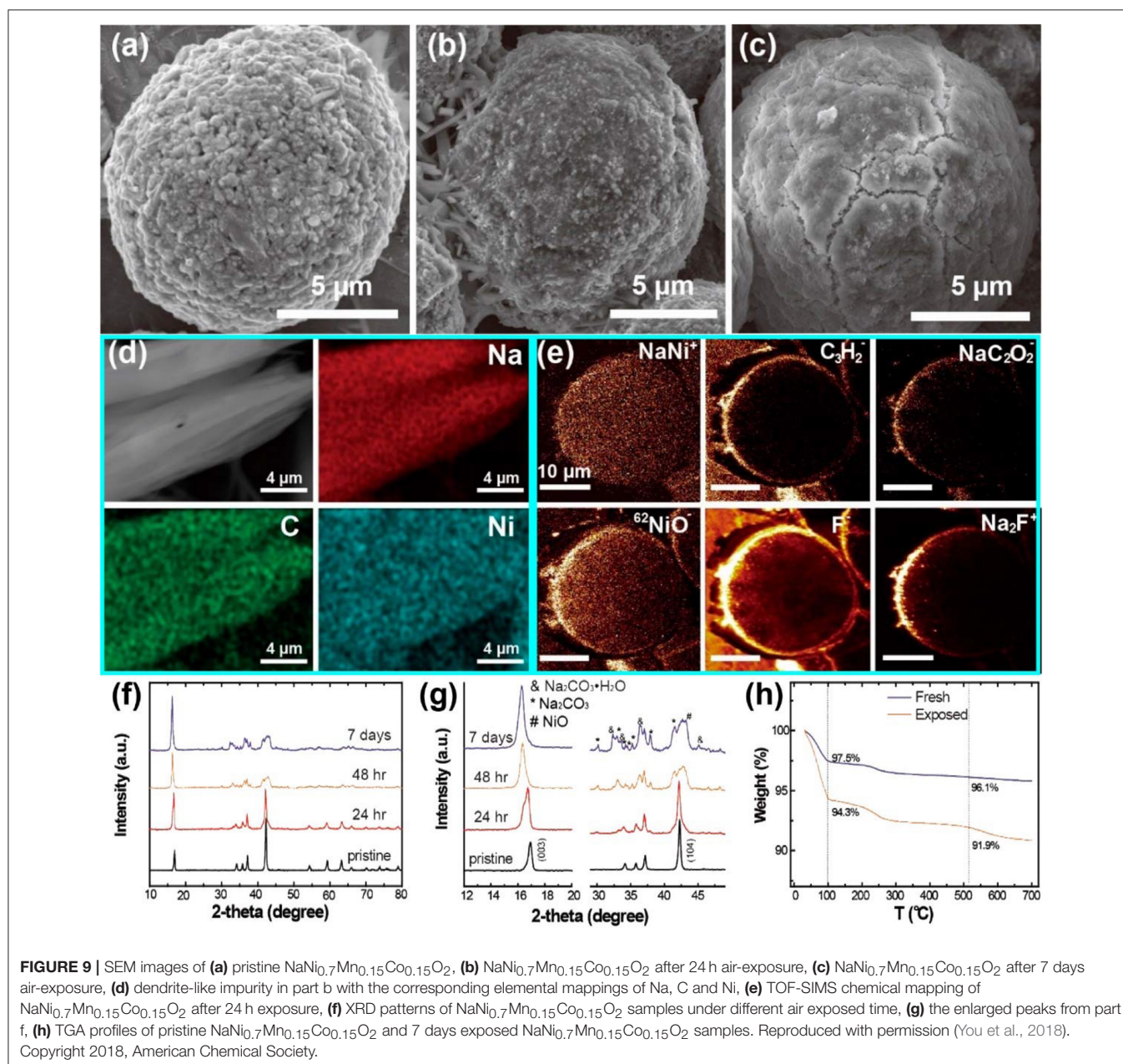
As mentioned above, NaOH is generated on the surface of O3 type Na<sub>x</sub>TMO<sub>2</sub> during the air exposure process, then CO<sub>2</sub> can further react with NaOH to form Na<sub>2</sub>CO<sub>3</sub> (Sathiya et al., 2012; Monyoncho and Bissessur, 2013; You et al., 2018). This reaction can be described as:



Sathiya et al. (2012) proved the formation of Na<sub>2</sub>CO<sub>3</sub> on the surface of NaNi<sub>1/3</sub>Mn<sub>1/3</sub>Co<sub>1/3</sub>O<sub>2</sub> particles. Compared to the pristine sample (Figure 7a), the surface showed no obvious change after 15 days air-exposure (Figure 7b) but became quite rough after 30 days air-exposure (Figure 7c). IR spectrum

revealed the bands of CO<sub>3</sub><sup>2-</sup> at 1,450 and 863 cm<sup>-1</sup>, suggesting the existence of sodium carbonates on NaNi<sub>1/3</sub>Mn<sub>1/3</sub>Co<sub>1/3</sub>O<sub>2</sub> particles' surface (Figure 7d). Monyoncho and Bissessur (2013) extracted the aqueous solution from the mixture of NaFeO<sub>2</sub> and water (Figure 7e). The XRD pattern of extracted sample matched very well to commercial Na<sub>2</sub>CO<sub>3</sub>, proving the reaction of CO<sub>2</sub> and NaFeO<sub>2</sub> compounds (Figure 7f).

After the formation of Na<sub>2</sub>CO<sub>3</sub> on the surface, the CO<sub>3</sub><sup>2-</sup> can even be inserted into the TM layer, forming a "CO<sub>4</sub>" tetrahedron. Duffort et al. elucidated the mechanism of CO<sub>3</sub><sup>2-</sup> insertion in Na<sub>0.67</sub>Mn<sub>0.5</sub>Fe<sub>0.5</sub>O<sub>2</sub> crystal (Duffort et al., 2015). With increasing the time of air exposure, ribbon-like particles start to appear and grow longer gradually



(Figures 8a–c). In addition, the corresponding XRD patterns of  $\text{Na}_{0.67}\text{Mn}_{0.5}\text{Fe}_{0.5}\text{O}_2$  are also changed. New peak is observed around  $13^\circ$  after a month air exposure (Figure 8d), indicating the formation of hydrate phase (phase 3) and sodium-depleted P2 phase (phase 2). In Fourier difference map, the existence of large residual nuclear density is caused by the carbonate ions (Figure 8e) because the insertion of  $\text{CO}_3^{2-}$  leading to the changing of the nuclear density distribution (Figure 9g). In the TM layer, the  $\text{CO}_3^{2-}$  is combined with one C-O bond to form a  $\text{CO}_4$  tetrahedron structure (Figure 8f).

Except for  $\text{Na}_2\text{CO}_3$ , other surface components are also observed. You et al. studied the surface reaction between  $\text{NaNi}_{0.7}\text{Mn}_{0.15}\text{Co}_{0.15}\text{O}_2$  and air systematically by using time-of-flight secondary ion mass spectroscopy (TOF-SIMS) (You et al., 2018). The pristine sample shows a microsphere morphology, which is consisted of nanosized particles (Figure 9a). After 24 h air exposure treatment, the surface of this microsphere becomes smooth with the absence of nano-particles (Figure 9b). Finally, a thick layer of impurities is formed on the surface after 7 days air exposure (Figure 9c). Elements of Na, Ni, and C are distributed uniformly on the impurity surface (Figure 9d). The existence of  $\text{NaNi}^+$ ,  $\text{NiO}$ ,  $\text{NaC}_2\text{O}_2^-$ ,  $\text{C}_3\text{H}_2^-$ ,  $\text{Na}_2\text{F}^+$ , and  $\text{F}^-$  composition are confirmed by TOF-SIMS, indicating the surface degradation of  $\text{NaNi}_{0.7}\text{Mn}_{0.15}\text{Co}_{0.15}\text{O}_2$  as well as the

reaction between sodium carbonates and PVDF (Figure 9e). The 003 peak shifts to lower angles gradually because of the migration of  $\text{Na}^+$  to the surface while the 104 peak becomes weak and vanishes after 48 h air exposure (Figure 9f). According to the XRD patterns in Figure 9g, impurities' peaks such as  $\text{NiO}$  and  $\text{Na}_2\text{CO}_3$  are observed, indicating the surface reaction when  $\text{NaNi}_{0.7}\text{Mn}_{0.15}\text{Co}_{0.15}\text{O}_2$  contacts to  $\text{CO}_2$  and  $\text{H}_2\text{O}$ . Since the  $\text{CO}_2$  and  $\text{H}_2\text{O}$  are absorbed and reacted with  $\text{NaNi}_{0.7}\text{Mn}_{0.15}\text{Co}_{0.15}\text{O}_2$ , the air-exposed sample loses more weight than the fresh sample (Figure 9h). All the results above can prove that  $\text{NaNi}_{0.7}\text{Mn}_{0.15}\text{Co}_{0.15}\text{O}_2$  can react with the water and carbon dioxide in the air and the impurities of  $\text{NaNi}^+$ ,  $\text{NiO}$ ,  $\text{NaC}_2\text{O}_2^-$ ,  $\text{C}_3\text{H}_2^-$ ,  $\text{Na}_2\text{F}^+$  and  $\text{F}^-$  are generated on the surface.

## AIR-STABLE $\text{Na}_x\text{TMO}_2$ COMPOUNDS

As mentioned above,  $\text{NaTMO}_2$  compounds can react with water and  $\text{CO}_2$  in air, which lead to: (i) the formation of impure phase on the surface; (ii) the insertion of  $\text{H}_2\text{O}$  and  $\text{CO}_3^{2-}$  into interlayer spacing and TM layers, respectively. On one side, the formed  $\text{NaOH}$  and  $\text{Na}_2\text{CO}_3$  impure phase are electrochemical inactive and have low conductivity hence the rate capability of  $\text{Na}_x\text{TMO}_2$  suffer serious decrease. On the other side, the water molecules can bring side reaction with electrolyte while the insertion of  $\text{CO}_3^{2-}$

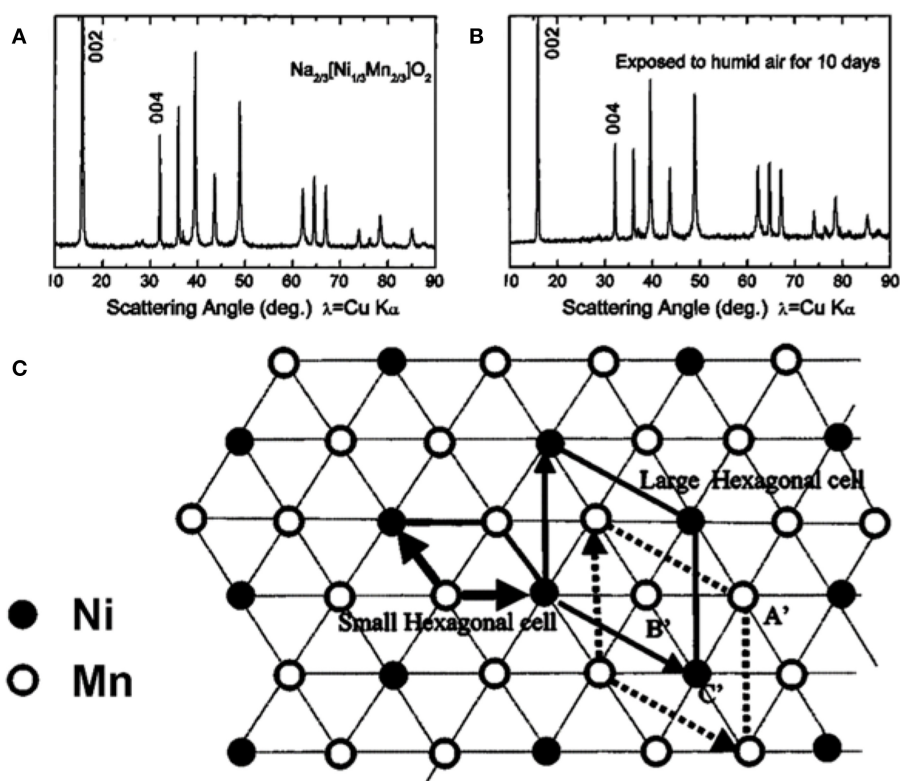


**FIGURE 10 | (A)** XRD pattern of pristine  $\text{Na}_{2/3}\text{Ni}_{1/3}\text{Mn}_{2/3}\text{O}_2$ . **(B)** XRD pattern of  $\text{Na}_{2/3}\text{Ni}_{1/3}\text{Mn}_{2/3}\text{O}_2$  after 10 days air-exposure. **(C)** the Ni/Mn cationic ordering arrangement. Reproduced with permission (Lu and Dahn, 2001b). Copyright 2001, American Chemical Society.

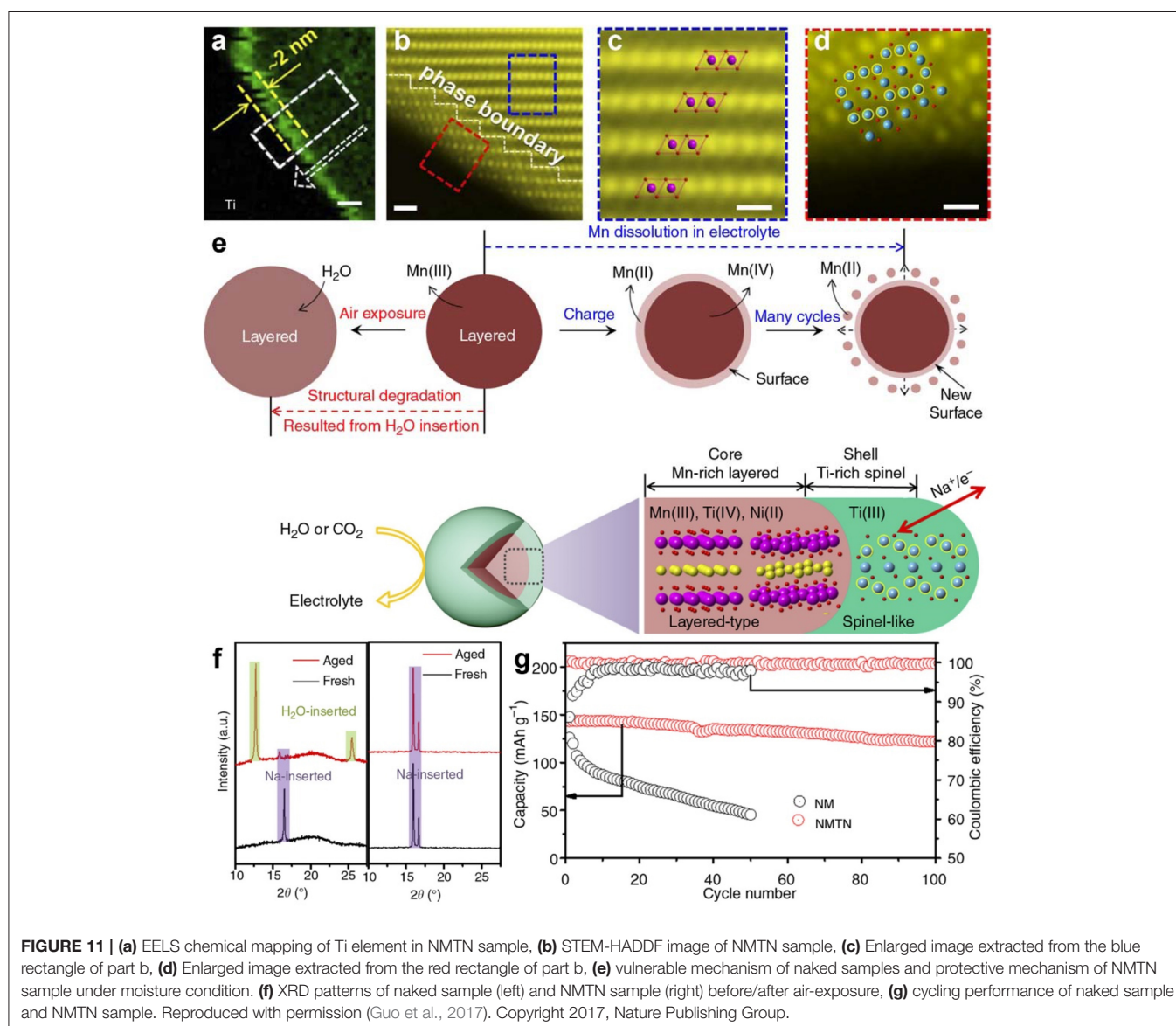
affects the valence state of TM ions, leading to severe capacity decay. Therefore, more and more researchers are focusing on strategies to address this air-instable problems.

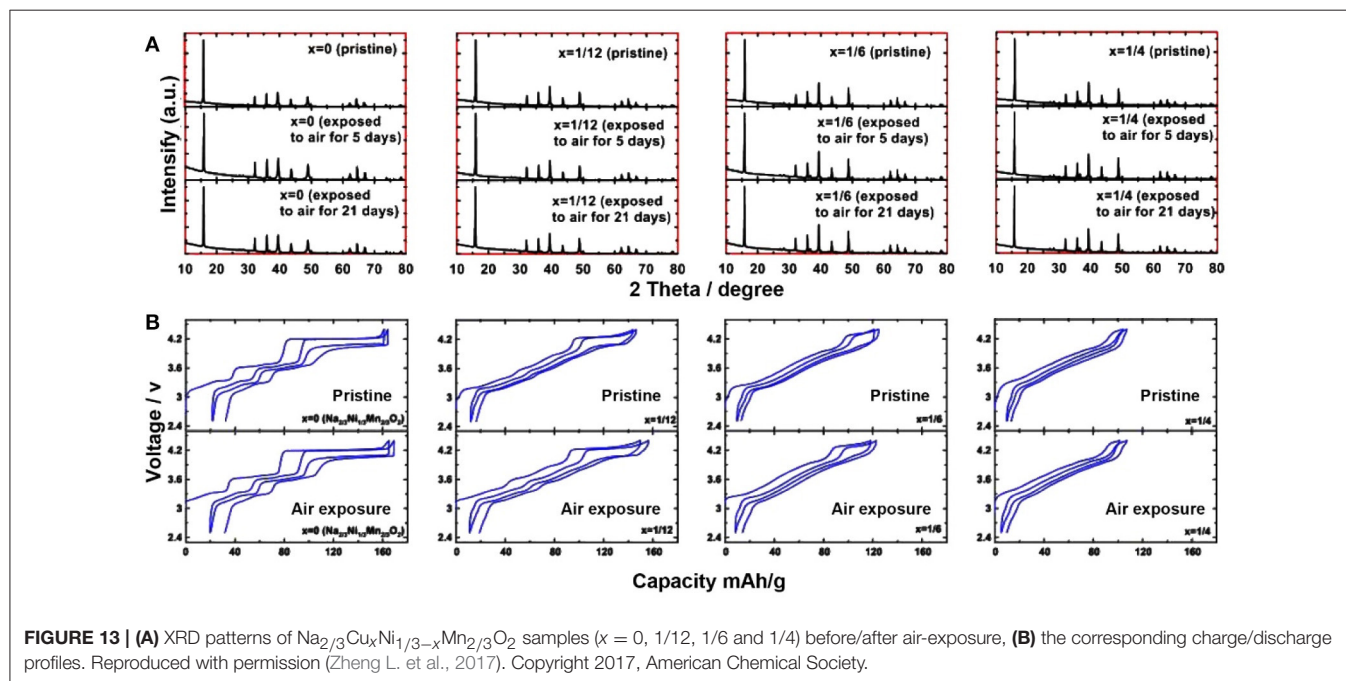
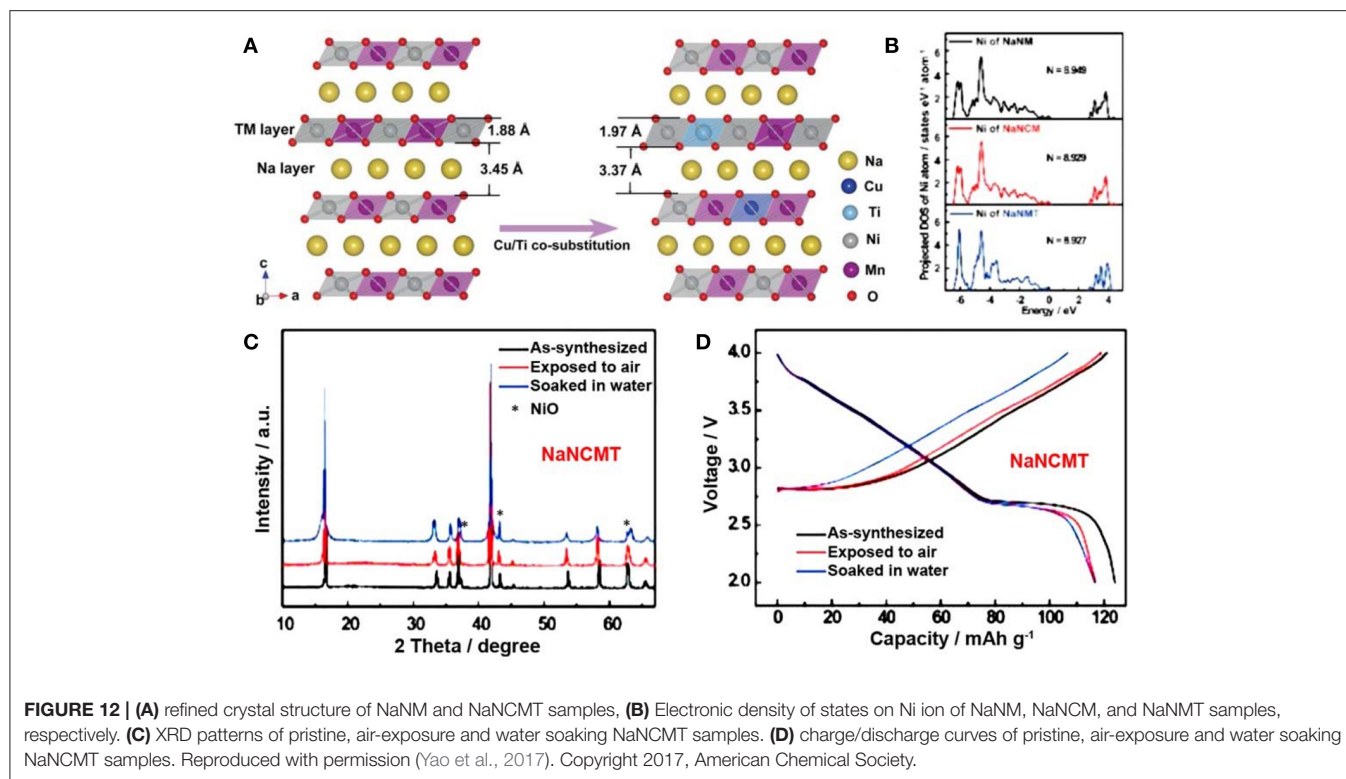
One strategy is to prevent the materials from contacting moisture. During the materials preparation process, once the high-temperature treatment is done, the  $\text{Na}_x\text{TMO}_2$  products are transferred to drying room (Wang et al., 2016a) or argon-filled glove box (Yabuuchi et al., 2012a; Vassilaras et al., 2014) immediately for the cooling process and subsequent cell assembling. However, this strategy may not be suitable for the large-scale application because huge cost will rise for materials' storage. Another strategy is to design air-stable  $\text{Na}_x\text{TMO}_2$  material. Recently, several P2 and O3 type  $\text{Na}_x\text{TMO}_2$  materials with high stability against moisture have been reported (Lu and Dahn, 2001b; Li Y. et al., 2015; Mu et al., 2015; Guo et al., 2017; Yao et al., 2017; Zheng L. et al., 2017; Chen et al., 2018; Deng et al., 2018). Under the treatment of air exposure and water

soaking, these air-stable cathodes can maintain their original crystal structure and electrochemical performance. In this part, several effective strategies for air-stable  $\text{Na}_x\text{TMO}_2$  designing are summarized.

## Constructing TM Cationic Ordering Arrangement

Lu et al. first reported an air-stable  $\text{P2-Na}_{2/3}\text{Ni}_{1/3}\text{Mn}_{2/3}\text{O}_2$  with high stability under moisture condition (Lu and Dahn, 2001b). For the  $\text{P2-Na}_{2/3}\text{Ni}_{1/3}\text{Mn}_{2/3}\text{O}_2$  sample, after undergoing a 10 days air-exposure treatment, no peaks shift or new peaks formation were observed in the XRD pattern, indicating that water could not be inserted into the interlayer spacing (Figures 10A,B). According to neutron diffraction analysis, the  $\text{Ni}^{2+}$  and  $\text{Mn}^{4+}$  ions formed an honeycomb structure with an  $\sqrt{3a} \times \sqrt{3a}$  ordering arrangement in the TM layers (Figure 10C) (Lu et al., 2000). This Ni/Mn ordering arrangement in TM





layers was supposed to induce a strong interlayer interaction to prevent the water insertion. When this ordering arrangement was suppressed by the substitution of Co or Fe for Ni, water molecules could be inserted into the interlayer spacing (Figures 5A,B,F). However, this “interlayer interaction” between adjacent ordering TM layer has not been confirmed yet.

## Coating Protective Layer

Coating a protective layer on the surface of  $\text{Na}_x\text{TMO}_2$  is an effective method to prevent the  $\text{Na}_x\text{TMO}_2$  from air contacting. The most common way is to coat high-voltage metal oxides with high stability against moisture. In 2017, Zhou and co-workers (Guo et al., 2017). designed an efficient

TABLE 2 | A summary of current air-stable  $\text{Na}_x\text{TMO}_2$  cathode.

Air stable materials	Design strategies	Test conditions	Rate performance			Cycling performance			References
			Maximum rate (C)	Capacity ( $\text{mAh g}^{-1}$ )	Capacity retention	Cycle rate (C)	Cycle number	Capacity retention	
$\text{Na}_{2/3}\text{Ni}_{1/3}\text{Mn}_{2/3}\text{O}_2$	Ni/Mn ordering arrangement	Air-exposure and water soaking	None	None	None	None	None	None	Lu and Dahn, 2001b
$\text{NaMnTi}_{0.1}\text{Ti}_{0.1}\text{O}_2$	titanium (III) oxides protective layer	Air-exposure	10	102	55%	5	500	81%	Guo et al., 2017
$\text{ZrO}_2@\text{NaNi}_{0.7}\text{Mn}_{0.15}\text{Co}_{0.15}\text{O}_2$	$\text{ZrO}_2$ protective layer	Air-exposure	10	41	37%	0.5	200	70%	You et al., 2018
$\text{NaNi}_{0.45}\text{Cu}_{0.05}\text{Mn}_{0.4}\text{Ti}_{0.1}\text{O}_2$	Cu/Ti co-substitution	Air-exposure and water soaking	4	100	80%	1	500	70.2%	Yao et al., 2017
$\text{Na}_{2/3}\text{Cu}_x\text{Ni}_{1/3-x}\text{Mn}_{2/3}\text{O}_2$	Cu substitution	Air-exposure	5	80	87%	None	None	None	Zheng L. et al., 2017
$\text{Na}_{7/9}\text{Cu}_{2/9}\text{Fe}_{1/9}\text{Mn}_{2/3}\text{O}_2$	Cu substitution	Air-exposure and water soaking	2	50	52%	1	150	87%	Li Y. et al., 2015
$\text{Na}_{0.9}\text{Cu}_{0.22}\text{Fe}_{0.30}\text{Mn}_{0.48}\text{O}_2$	Cu substitution	Air-exposure	5	60	60%	0.1	100	97%	Mu et al., 2015
$\text{NaNi}_{0.05}\text{Mn}_{0.5}\text{Ni}_{0.3}\text{Cu}_{0.1}\text{Mg}_{0.05}\text{O}_2$	Cu substitution	Water soaking	1	125	71%	1	400	67.4%	Deng et al., 2018
$\text{Na}_{0.6}\text{Mn}_{0.9}\text{Cu}_{0.1}\text{O}_2$	Cu substitution	Air-exposure and water soaking	8	85	50.4%	4	250	70.4%	Chen et al., 2018

spinel-like titanium (III) oxides protective interface to improve the structure/electrochemical stability of  $\text{NaNiTi}_{0.1}\text{Ni}_{0.1}\text{O}_2$ . The sample surface was covered by a high Ti concentration layer with thickness of 2 nm, as shown in the electron energy-loss spectroscopy image (Figure 11a). Two distinct phases could be observed from the high-angle annular dark field scanning transmission electron microscopy (HAADF-STEM) image (Figure 11b). The bulk phase was a typical layered structure (Figure 11c) while the surface phase was spinel-like structure (Figures 11d,e). After exposing the naked bulk phase in humid air, two new peaks appeared around  $12^\circ$  and  $25^\circ$  (Figure 11f), indicating the insertion of water molecules. Compared to the naked bulk phase, the XRD pattern of  $\text{NaNiTi}_{0.1}\text{Ni}_{0.1}\text{O}_2$  sample showed no peak change since the spinel-like titanium (III) oxides interface can act as shield to protect the bulk phase from water attacking and the electrochemical performance of bulk phase can be maintained. In half cell system, the naked bulk phase showed a dramatic decrease after 50 cycles whereas NMTN sample only showed a slight decay after 100 cycles (Figure 11g).

You et al. (2018) coated the surface of  $\text{NaNi}_{0.7}\text{Mn}_{0.15}\text{Co}_{0.15}\text{O}_2$  with a  $\text{ZrO}_2$  protective layer. This protective layer notably maintains the rate capability of  $\text{NaNi}_{0.7}\text{Mn}_{0.15}\text{Co}_{0.15}\text{O}_2$  against moisture atmosphere. After 7 days air exposure, the  $\text{ZrO}_2@\text{NaNi}_{0.7}\text{Mn}_{0.15}\text{Co}_{0.15}\text{O}_2$  sample still delivers a capacity of 96 mAh/g while  $\text{NaNi}_{0.7}\text{Mn}_{0.15}\text{Co}_{0.15}\text{O}_2$  shows abnormal charge profile. The surface charge-transfer kinetics are also improved by this protective layer.

Except for Ti and Zr oxides, we suppose that other metal oxides such as  $\text{MgO}$ ,  $\text{ZnO}$ , and  $\text{Al}_2\text{O}_3$  also have the ability to work as protective layer because these high-voltage metal oxides all have high tolerance for moisture.

## Cu<sup>2+</sup> Substitution

The Cu<sup>2+</sup> substitution is the simplest way to obtain air-stable  $\text{Na}_x\text{TMO}_2$  compounds. The success of Cu<sup>2+</sup> substitution to achieve high stability against moisture has been proven by many reports (Li Y. et al., 2015; Mu et al., 2015; Yao et al., 2017; Zheng L. et al., 2017; Chen et al., 2018; Deng et al., 2018), few references give the working mechanisms of Cu<sup>2+</sup> in these air-stable  $\text{Na}_x\text{TMO}_2$  compounds.

In, 2017, Yao et al. designed an air-stable  $\text{O3-NaNi}_{0.45}\text{Cu}_{0.05}\text{Mn}_{0.4}\text{Ti}_{0.1}\text{O}_2$  (NaNcMT) cathode though cosubstitution of Cu<sup>2+</sup> and Ti<sup>4+</sup> in  $\text{O3-NaNi}_{0.5}\text{Mn}_{0.5}\text{O}_2$  (NaNM) compound. This strategy could decrease the Na<sup>+</sup> interlayer distance and increase the valence state of TM ions. According to the refined crystal structure of NaNM and NaNcMT, the interlayer distance was reduced from 3.45 Å to 3.37 Å, respectively (Figure 12A), which was in favor of preventing the insertion of water molecules. DFT calculation revealed that Cu/Ti cosubstitution facilitated the increasing in valence state of Ni (Figure 12B). Compared with NaNM compound (Figure 6B), the XRD pattern of NaNcMT sample showed no obvious peaks change after air-exposure or water soaking (Figure 12C). During charge/discharge process, only slight capacity decay was observed after aging experiments (Figure 12D). (Yao et al., 2017) However, the explanation

about the relationship between valence state of TM ions and air-stability was not mentioned.

Zheng et al. investigated the structure stability of  $\text{Na}_{2/3}\text{Cu}_x\text{Ni}_{1/3-x}\text{Mn}_{2/3}\text{O}_2$  compounds ( $0 \leq x \leq 1/4$ ) by air-exposure treatment. Compared to the XRD patterns of pristine samples, neither peaks position change nor new peaks formation were observed after exposing  $\text{Na}_{2/3}\text{Cu}_x\text{Ni}_{1/3-x}\text{Mn}_{2/3}\text{O}_2$  in air condition for 21 days (Figure 13A). According to charge/discharge profiles, all exposed electrodes had a little higher open circuit voltage than the un-exposed electrodes, but the average voltage and reversible capacity of the exposed electrodes showed no change or decay, indicating the air stability of these electrodes (Figure 13B). Since the radii of  $\text{Cu}^{2+}$  (0.73 Å) and  $\text{Ni}^{2+}$  (0.69 Å) were similar, replacing  $\text{Ni}^{2+}$  in  $\text{Na}_{2/3}\text{Ni}_{1/3}\text{Mn}_{2/3}\text{O}_2$  by  $\text{Cu}^{2+}$  had no influence on the Ni/Mn cationic ordering arrangement. Therefore, the existence of Cu/Ni/Mn ordering arrangement could prevent the insertion of water molecules into the  $\text{Na}_{2/3}\text{Cu}_x\text{Ni}_{1/3-x}\text{Mn}_{2/3}\text{O}_2$  interlayer spacing because of the interlayer interaction between the adjacent Cu/Ni/Mn layer. However, no evidence was provided to prove the Cu/Ni/Mn ordering arrangement.

Other compounds such as  $\text{O}_3\text{-Na}_{0.9}\text{Cu}_{0.22}\text{Fe}_{0.30}\text{Mn}_{0.48}\text{O}_2$ ,  $\text{P}_2\text{-Na}_{7/9}\text{Cu}_{2/9}\text{Fe}_{1/9}\text{Mn}_{2/3}\text{O}_2$ ,  $\text{O}_3\text{-NaLi}_{0.05}\text{Mn}_{0.5}\text{Ni}_{0.3}\text{Cu}_{0.1}\text{Mg}_{0.05}\text{O}_2$ , and  $\text{P}_2\text{-Na}_{0.6}\text{Mn}_{0.9}\text{Cu}_{0.1}\text{O}_2$  have been proved to be air-stable because all of their XRD patterns remained unchanged after air-exposure and water soaking treatment (Li Y. et al., 2015; Mu et al., 2015; Chen et al., 2018; Deng et al., 2018).

It seems that the  $\text{Cu}^{2+}$  plays an important role in maintaining the structure stability of these compounds under moisture. The reported  $\text{Cu}^{2+}$  substituted  $\text{Na}_x\text{TMO}_2$  compounds, such as  $\text{O}_3\text{-NaNi}_{0.45}\text{Cu}_{0.05}\text{Mn}_{0.4}\text{Ti}_{0.1}\text{O}_2$ ,  $\text{P}_2\text{-Na}_{2/3}\text{Cu}_x\text{Ni}_{1/3-x}\text{Mn}_{2/3}\text{O}_2$ ,  $\text{O}_3\text{-Na}_{0.9}\text{Cu}_{0.22}\text{Fe}_{0.30}\text{Mn}_{0.48}\text{O}_2$ ,  $\text{O}_3\text{-NaLi}_{0.05}\text{Mn}_{0.5}\text{Ni}_{0.3}\text{Cu}_{0.1}\text{Mg}_{0.05}\text{O}_2$ ,  $\text{P}_2\text{-Na}_{7/9}\text{Cu}_{2/9}\text{Fe}_{1/9}\text{Mn}_{2/3}\text{O}_2$ , and  $\text{P}_2\text{-Na}_{0.6}\text{Mn}_{0.9}\text{Cu}_{0.1}\text{O}_2$ , all show excellent structure stability under moisture condition. However, few investigations explain the working mechanism of  $\text{Cu}^{2+}$  substitution in these air-stable compounds. In  $\text{O}_3\text{-NaNi}_{0.45}\text{Cu}_{0.05}\text{Mn}_{0.4}\text{Ti}_{0.1}\text{O}_2$  compound system, the working mechanism of  $\text{Cu}^{2+}$  is attributed to the increase of the

Ni valence state by DFT calculation, but the relationship between valence state of Ni and air-stability is not clear so far. In addition, how to explain the Ni free compound systems for their air stability after  $\text{Cu}^{2+}$  substitution still remains problems.

Table 2 lists most of the air-stable  $\text{Na}_x\text{TMO}_2$  compounds published to date, including the design strategies and the corresponding electrochemical performance.

## SUMMARY AND PROSPECTS

Air-stability is one of the key issues for practical application of  $\text{Na}_x\text{TMO}_2$  SIB cathode materials. In recent years, with understanding the structure of  $\text{Na}_x\text{TMO}_2$ , several strategies have been developed to obtain air-stable  $\text{Na}_x\text{TMO}_2$  compounds, including constructing TM ordering arrangement, coating protective layer and  $\text{Cu}^{2+}$  substitution. However, there still remain some challenges. For example, the reaction mechanism of the “strong interlayer interaction” for TM ordering arrangement as well as the substitution of  $\text{Cu}^{2+}$  and other cations should be further understood. In any case, we believe that the air-stable  $\text{Na}_x\text{TMO}_2$  materials with low cost and high theoretical capacity are highly competitive as SIB cathode materials in the large-scale energy storage application.

## AUTHOR CONTRIBUTIONS

RZ contributed conception and design of the manuscript. YZ organized the reference and wrote the first draft of the manuscript. All authors contributed to manuscript revision, read and approved the submitted version.

## ACKNOWLEDGMENTS

We gratefully acknowledge the financial support from the National Natural Science Foundation of China (Nos. 51602221 and 51632001), Shanghai Municipal Natural Science Foundation (16ZR1438400) and the Fundamental Research Funds for the Central Universities.

## REFERENCES

- Ado, K., Tabuchi, M., Kobayashi, H., Kageyama, H., Nakamura, O., Inaba, Y., et al. (1997). Preparation of  $\text{LiFeO}_2$  with Alpha- $\text{NaFeO}_2$ -type structure using a mixed-alkaline hydrothermal method. *J. Electrochem. Soc.* 144, L177–L180.
- Arachi, Y., Setsu, T., Ide, T., Hinoshita, K., and Nakata, Y. (2012). Reversible electrochemical reaction of CuO with Li in the  $\text{LiCuO}_2$  system. *Solid State Ionics* 225, 611–614. doi: 10.1016/j.ssi.2011.12.006
- Bai, X., Sathiyaa, M., Mendoza-Sánchez, B., Iadecola, A., Vergnet, J., Dedryvère, R., et al. (2018). Anionic redox activity in a newly Zn-doped sodium layered oxide  $\text{P}_2\text{-Na}_{2/3}\text{Mn}_{1-y}\text{Zn}_y\text{O}_2$  ( $0 < y < 0.23$ ). *Adv. Energy Mater.* 8:1802379. doi: 10.1002/aenm.201802379
- Benedek, R., and van de Walle, A. (2008). Free energies for acid attack reactions of lithium cobaltate. *J. Electrochem. Soc.* 155, A711–A715. doi: 10.1149/1.2954958
- Berthelot, R., Carlier, D., and Delmas, C. (2011). Electrochemical investigation of the  $\text{P}_2\text{-Na}_x\text{CoO}_2$  phase diagram. *Nat. Mater.* 10, 74–80. doi: 10.1038/nmat2920
- Blesa, M. C., Morán, E., Menéndez, N., Tornero, J. D., and Torrón, C. (1993). Hydrolysis of sodium orthoferrite [ $\alpha\text{-NaFeO}_2$ ]. *Mater. Res. Bull.* 28, 837–847. doi: 10.1016/0025-5408(93)90025-9
- Blyr, A., Sigala, C., Amatucci, G., Guyomard, D., Chabre, Y., Tarascon, J., et al. (1998). Self-discharge of  $\text{LiMn}_2\text{O}_4/\text{C}$  Li-Ion cells in their discharged state: understanding by means of three-electrode measurements. *J. Electrochem. Soc.* 145, 194–209. doi: 10.1149/1.1838235
- Boyd, S., Dhall, R., LeBeau, J., and Augustyn, V. (2018). Charge storage mechanism and degradation of  $\text{P}_2$ -type sodium transition metal oxides in aqueous electrolytes. *J. Mater. Chem. A* 6, 22266–22276. doi: 10.1039/C8TA08367C
- Braconnier, J. J., Delmas, C., and Hagenmuller, P. (1982). Etude par desintercalation électrochimique des systèmes  $\text{Na}_x\text{CrO}_2$  et  $\text{Na}_x\text{NiO}_2$ . *Mater. Res. Bull.* 17, 993–1000. doi: 10.1016/0025-5408(82)90124-6
- Bucher, N., Hartung, S., Franklin, J. B., Wise, A. M., Lim, L. M., Chen H.-Y., et al. (2016).  $\text{P}_2\text{-Na}_x\text{Co}_y\text{Mn}_{1-y}\text{O}_2$  ( $y = 0, 0.1$ ) as cathode materials in sodium-ion

- batteries—effects of doping and morphology to enhance cycling stability. *Chem. Mater.* 28, 2041–2051. doi: 10.1021/acs.chemmater.5b04557
- Buchholz, D., Chagas, L. G., Vaalma, C., Wu, L., and Passerini, S. (2014). Water sensitivity of layered P2/P3-Na<sub>x</sub>Ni<sub>0.22</sub>Co<sub>0.11</sub>Mn<sub>0.66</sub>O<sub>2</sub> cathode material. *J. Mater. Chem. A* 2, 13415–13421. doi: 10.1039/C4TA02627F
- Caballero, A., Hernan, L., Morales, J., Sanchez, L., Pena, J. S., Aranda, M. A. G., et al. (2002). Synthesis and characterization of high-temperature hexagonal P2-Na<sub>0.6</sub>MnO<sub>2</sub> and its electrochemical behaviour as cathode in sodium cells. *J. Mater. Chem.* 12, 1142–1147. doi: 10.1039/b108830k
- Carlier, D., Cheng, J. H., Berthelot, R., Guignard, M., Yoncheva, M., Stoyanova, R., et al. (2011). The P2-Na<sub>2/3</sub>Co<sub>2/3</sub>Mn<sub>1/3</sub>O<sub>2</sub> phase: structure, physical properties and electrochemical behavior as positive electrode in sodium battery. *Dalton Trans.* 40, 9306–9312. doi: 10.1039/c1dt10798d
- Chen, T. R., Sheng, T., Wu, Z. G., Li, J. T., Wang, E.-H., Wu, C.-H., et al. (2018). Cu<sup>(2+)</sup> dual-doped layer-tunnel hybrid Na<sub>0.6</sub>Mn<sub>1-x</sub>Cu<sub>x</sub>O<sub>2</sub> as a cathode of sodium-ion battery with enhanced structure stability, electrochemical property, and air stability. *ACS Appl. Mater. Interfaces* 10, 10147–10156. doi: 10.1021/acsami.8b00614
- Chen, X., Zhou, X., Hu, M., Liang, J., Wu, D., Wei, J., et al. (2015). Stable layered P3/P2 Na<sub>0.66</sub>Co<sub>0.5</sub>Mn<sub>0.5</sub>O<sub>2</sub> cathode materials for sodium-ion batteries. *J. Mater. Chem. A* 3, 20708–20714. doi: 10.1039/C5TA05205J
- Delmas, C., Braconnier, J.-J., Fouassier, C., and Hagenmuller, P. (1981). Electrochemical intercalation of sodium in Na<sub>x</sub>CoO<sub>2</sub> bronzes. *Solid State Ionics* 3, 165–169. doi: 10.1016/0167-2738(81)90076-X
- Delmas, C., Fouassier, C., and Hagenmuller, P. (1980). Structural classification and properties of the layered oxides. *Physica B+C* 99, 81–85. doi: 10.1016/0378-4363(80)90214-4
- Deng, J., Luo, W.-B., Lu, X., Yao, Q., Wang, Z., Liu, H.-K., et al. (2018). High energy density sodium-ion battery with industrially feasible and air-stable O3-type layered oxide cathode. *Adv. Energy Mater.* 8:1701610. doi: 10.1002/aenm.201701610
- Duffort, V., Talaie, E., Black, R., and Nazar, L. F. (2015). Uptake of CO<sub>2</sub> in layered P2-Na<sub>0.67</sub>Mn<sub>0.5</sub>Fe<sub>0.5</sub>O<sub>2</sub> insertion of carbonate anions. *Chem. Mater.* 27, 2515–2524. doi: 10.1021/acs.chemmater.5b00097
- Dunn, B., Kamath, H., and Tarascon, J.-M. (2011). Electrical energy storage for the grid: a battery of choices. *Science* 334, 928–935. doi: 10.1126/science.1212741
- Fang, C., Huang, Y., Yuan, L., Liu, Y., Chen, W., Huang, Y., et al. (2017). A metal-organic compound as cathode material with superhigh capacity achieved by reversible cationic and anionic redox chemistry for high-energy sodium-ion batteries. *Angew. Chem. Int. Ed.* 56, 6793–6797. doi: 10.1002/anie.201701213
- Fielden, R., and Obrovac, M. N. (2015). Investigation of the NaNi<sub>x</sub>Mn<sub>1-x</sub>O<sub>2</sub> (0 <= x <= 1) system for na-ion battery cathode materials. *J. Electrochem. Soc.* 162, A453–A459. doi: 10.1149/2.0551503jes
- Franger, S., Bach, S., Pereira-Ramos, J. P., and Baffier, N. (2000). Chemistry and electrochemistry of low-temperature manganese oxides as lithium intercalation compounds. *J. Electrochem. Soc.* 147, 3226–3230. doi: 10.1149/1.1393887
- Gonzalo, E., Han, M. H., del Amo, J. M. L., Acebedo, B., Casas-Cabanas, M., Rojo, T., et al. (2014). Synthesis and characterization of pure P2-and O3-Na<sub>2/3</sub>Fe<sub>2/3</sub>Mn<sub>1/3</sub>O<sub>2</sub> as cathode materials for Na ion batteries. *J. Mater. Chem. A* 2, 18523–18530. doi: 10.1039/C4TA03991B
- Guignard, M., Didier, C., Darriet, J., Bordet, P., Elkaim, E., and Delmas, C. (2013). P2-Na<sub>x</sub>VO<sub>2</sub> system as electrodes for batteries and electron-correlated materials. *Nat Mater.* 12, 74–80. doi: 10.1038/nmat3478
- Guo, S., Li, Q., Liu, P., Chen, M., and Zhou, H. (2017). Environmentally stable interface of layered oxide cathodes for sodium-ion batteries. *Nat. Commun.* 8:135. doi: 10.1038/s41467-017-00157-8
- Guo, S., Yu, H., Liu, D., Tian, W., Liu, X., Hanada, N., et al. (2014). A novel tunnel Na<sub>0.61</sub>Ti<sub>0.48</sub>Mn<sub>0.52</sub>O<sub>2</sub> cathode material for sodium-ion batteries. *Chem. Commun.* 50, 7998–8001. doi: 10.1039/c4cc02362e
- Hamani, D., Ati, M., Tarascon, J.-M., and Rozier, P. (2011). Na<sub>x</sub>VO<sub>2</sub> as possible electrode for Na-ion batteries. *Electrochem. Commun.* 13, 938–941. doi: 10.1016/j.elecom.2011.06.005
- Han, M. H., Gonzalo, E., Sharma, N. J., López del Amo, M., Armand, M., Avdeev, M., et al. (2016a). High-performance P2-phase Na<sub>2/3</sub>Mn<sub>0.8</sub>Fe<sub>0.1</sub>Ti<sub>0.1</sub>O<sub>2</sub> cathode material for ambient-temperature sodium-ion batteries. *Chem. Mater.* 28, 106–116. doi: 10.1021/acs.chemmater.5b03276
- Han, M. H., Gonzalo, E., Singh, G., and Rojo, T. (2015). A comprehensive review of sodium layered oxides: powerful cathodes for Na-ion batteries. *Energy Environ. Sci.* 8, 81–102. doi: 10.1039/C4EE03192J
- Han, M. H., Sharma, N., Gonzalo, E., Pramudita, J. C., Brand, H. E., et al. (2016b). Moisture exposed layered oxide electrodes as Na-ion battery cathodes. *J. Mater. Chem. A* 4, 18963–18975. doi: 10.1039/C6TA07950D
- Hwang, J.-Y., Myung, S.-T., and Sun, Y.-K. (2017). Sodium-ion batteries: present and future. *Chem. Soc. Rev.* 46, 3529–3614. doi: 10.1039/C6CS00776G
- Jiang, K., Xu, S., Guo, S., Zhang, X., Zhang, X., Qiao, Y., et al. (2018). A phase-transition-free cathode for sodium-ion batteries with ultralong cycle life. *Nano Energy* 52, 88–94. doi: 10.1016/j.nanoen.2018.07.042
- Jiang, X., Liu, S., Xu, H., Chen, L., Yang, J., and Qian, Y. (2015). Tunnel-structured Na<sub>0.54</sub>Mn<sub>0.50</sub>Ti<sub>0.51</sub>O<sub>2</sub> and Na<sub>0.54</sub>Mn<sub>0.50</sub>Ti<sub>0.51</sub>O<sub>2</sub>/C nanorods as advanced cathode materials for sodium-ion batteries. *Chem. Commun.* 51, 8480–8483. doi: 10.1039/C5CC02233A
- Kalluri, S., Seng, K. H., Pang, W. K., Guo, Z., Chen, Z., Liu H. K., et al. (2014). Electrospun P2-type Na<sub>2/3</sub>Fe<sub>1/2</sub>Mn<sub>1/2</sub>O<sub>2</sub> hierarchical nanofibers as cathode material for sodium-ion batteries. *ACS Appl. Mater. Interfaces* 6, 8953–8958. doi: 10.1021/am502343s
- Kang, S. M., Park, J.-H., Jin, A., Jung, Y. H., Mun, J., Sung, Y.-E. (2018). Na<sup>+</sup>/vacancy disordered P2-Na<sub>0.67</sub>Co<sub>1-x</sub>Ti<sub>x</sub>O<sub>2</sub>: high-energy and high-power cathode materials for sodium ion batteries. *ACS Appl. Mater. Interfaces* 10, 3562–3570. doi: 10.1021/acsami.7b16077
- Kang, W., Yu, D. Y., Lee, P.-K., Zhang, Z., Bian, H., Li, W., et al. (2016). P2-Type Na<sub>x</sub>Cu<sub>0.15</sub>Ni<sub>0.20</sub>Mn<sub>0.65</sub>O<sub>2</sub> cathodes with high voltage for high-power and long-life sodium-ion batteries. *ACS Appl. Mater. Interfaces* 8, 31661–31668. doi: 10.1021/acsami.6b10841
- Kang, W., Zhang, Z., Lee, P.-K., Ng, T.-W., Li, W., Tang, Y., et al. (2015). Copper substituted P2-type Na<sub>0.67</sub>Cu<sub>x</sub>Mn<sub>1-x</sub>O<sub>2</sub>: a stable high-power sodium-ion battery cathode. *J. Mater. Chem. A* 3, 22846–22852. doi: 10.1039/C5TA06371J
- Kawamura, T., Okada, S., and Yamaki, J.-I. (2006). Decomposition reaction of LiPF<sub>6</sub>-based electrolytes for lithium ion cells. *J. Power Sources* 156, 547–554. doi: 10.1016/j.jpowsour.2005.05.084
- Kee, Y., Dimov, N., Champet, S., Gregory, D. H., and Okada, S. (2016). Investigation of Al-doping effects on the NaFe<sub>0.5</sub>Mn<sub>0.5</sub>O<sub>2</sub> cathode for Na-ion batteries. *Ionics* 22, 2245–2248. doi: 10.1007/s11581-016-1839-2
- Kim, D., Cho, M., and Cho, K. (2017). Rational design of Na(Li<sub>1/3</sub>Mn<sub>2/3</sub>)O<sub>2</sub> operated by anionic redox reactions for advanced sodium-ion batteries. *Adv Mater* 29:1701788. doi: 10.1002/adma.201701788
- Kubota, K., and Komaba, S. (2015). Review—practical issues and future perspective for Na-Ion batteries. *J. Electrochem. Soc.* 162, A2538–A2550. doi: 10.1149/2.0151514jes
- Kundu, D., Talaie, E., Duffort, V., and Nazar, L. F. (2015). The emerging chemistry of sodium ion batteries for electrochemical energy storage. *Angew. Chem. Int. Ed. Engl.* 54, 3431–3448. doi: 10.1002/anie.201410376
- Le Goff, P., Baffier, N., Bach, S., Pereira-Ramos, J. P., and Messina, R. (1993). Structural and electrochemical characteristics of a lamellar sodium manganese oxide synthesized via a sol-gel process. *Solid State Ionics* 61, 309–315. doi: 10.1016/0167-2738(93)90397-L
- Li, X., Wu, D., Zhou, Y. N., Liu, L., Yang, X.-Q., Ceder, G., et al. (2014). O3-type Na(Mn<sub>0.25</sub>Fe<sub>0.25</sub>Co<sub>0.25</sub>Ni<sub>0.25</sub>)O<sub>2</sub>: a quaternary layered cathode compound for rechargeable Na ion batteries. *Electrochem. Commun.* 49, 51–54. doi: 10.1016/j.elecom.2014.10.003
- Li, Y., Yang, Z., Xu, S., Mu, L., Gu, L., Hu, Y.-S., et al. (2015). Air-stable copper-based P2-Na<sub>7/9</sub>Cu<sub>2/9</sub>Fe<sub>1/9</sub>Mn<sub>2/3</sub>O<sub>2</sub> as a new positive electrode material for sodium-ion batteries. *Adv. Sci.* 2:1500031. doi: 10.1002/adv.201500031
- Li, Z.-Y., Gao, R., Sun, L., Hu, Z., and Liu, X. (2015). Designing an advanced P2-Na<sub>0.67</sub>Mn<sub>0.65</sub>Ni<sub>0.2</sub>Co<sub>0.15</sub>O<sub>2</sub> layered cathode material for Na-ion batteries. *J. Mater. Chem. A* 3, 16272–16278. doi: 10.1039/C5TA02450A
- Liu, L., Li, X., Bo, S.-H., Wang, Y., Chen, H., Twu, N., et al. (2015). High-performance P2-type Na<sub>2/3</sub>(Mn<sub>1/2</sub>Fe<sub>1/4</sub>Co<sub>1/4</sub>)O<sub>2</sub> cathode material with superior rate capability for Na-Ion batteries. *Adv. Energy Mater.* 5:1500944. doi: 10.1002/aenm.201500944
- Liu, Y., Fang, X., Zhang, A., Shen, C., Liu, Q., Enaya, H., et al. (2016). Layered P2-Na<sub>2/3</sub>[Ni<sub>1/3</sub>Mn<sub>2/3</sub>]O<sub>2</sub> as high-voltage cathode for sodium-ion batteries: the capacity decay mechanism and Al<sub>2</sub>O<sub>3</sub> surface modification. *Nano Energy* 27, 27–34. doi: 10.1016/j.nanoen.2016.06.026
- Lu, Z., and Dahn, J. R. (2001a). *In situ* X-ray diffraction study of P2-Na<sub>2/3</sub>[Ni<sub>1/3</sub>Mn<sub>2/3</sub>]O<sub>2</sub>. *J. Electrochem. Soc.* 148, A1225–A1229. doi: 10.1149/1.1407247

- Lu, Z., and Dahn, J. R. (2001b). Intercalation of water in P2, T2 and O2 structure  $A_z[Co_xNi_{1/3-x}Mn_{2/3}]O_2$ . *Chem. Mater.* 13, 1252–1257. doi: 10.1021/cm000721x
- Lu, Z., Donaberger, R. A., and Dahn, J. R. (2000). Superlattice ordering of Mn, Ni, and Co in layered alkali transition metal oxides with P2, P3, and O3 structures. *Chem. Mater.* 12, 3583–3590. doi: 10.1021/cm000359m
- Luo, W., Chen, X., Xia, Y., Chen, M., Wang, L., Wang, Q., et al. (2017). Surface and interface engineering of silicon-based anode materials for lithium-ion batteries. *Adv. Energy Mater.* 7:1701083. doi: 10.1002/aenm.201701083
- Lux, S. F., Lucas, I. T., Pollak, E., Passerini, S., Winter, M., Kostecki, R. (2012). The mechanism of HF formation in LiPF<sub>6</sub> based organic carbonate electrolytes. *Electrochem. Commun.* 14, 47–50. doi: 10.1016/j.elecom.2011.10.026
- Ma, X., Chen, H., and Ceder, G. (2011). Electrochemical properties of monoclinic  $NaMnO_2$ . *J. Electrochem. Soc.* 158, A1307–A1312. doi: 10.1149/2.035112jes
- Maitra, U., House, R. A., Somerville, J. W., Tapia-Ruiz, N., Lozano, J. G., Guerrini, N., et al. (2018). Oxygen redox chemistry without excess alkali-metal ions in  $Na_{2/3}[Mg_{0.28}Mn_{0.72}]O_2$ . *Nat. Chem.* 10:288. doi: 10.1038/nchem.2923
- Manikandan, P., Heo, S., Kim, H. W., Jeong, H. Y., Lee, E., and Kim, Y. (2017). Structural characterization of layered  $Na_{0.5}Co_{0.5}Mn_{0.5}O_2$  material as a promising cathode for sodium-ion batteries. *J. Power Sources* 363, 442–449. doi: 10.1016/j.jpowsour.2017.07.116
- Monyoncho, E., and Bissessur, R. (2013). Unique properties of  $\alpha$ - $NaFeO_2$ : De-intercalation of sodium via hydrolysis and the intercalation of guest molecules into the extract solution. *Mater. Res. Bull.* 48, 2678–2686. doi: 10.1016/j.materresbull.2013.03.027
- Morris, D. J. P., Roger, M., Gutmann, M. J., Goff, J. P., Tennant, D. A., Prabhakaran, D., et al. (2009). Crystal-to-stripe reordering of sodium ions in  $Na_xCoO_2$ . *Phys. Rev. B* 79:100103. doi: 10.1103/PhysRevB.79.100103
- Mortemard de Boisse, B., Carlier, D., Guignard, M., and Delmas, C. (2013). Structural and electrochemical characterizations of P2 and new O3- $Na_xMn_{1-y}Fe_yO_2$  phases prepared by auto-combustion synthesis for Na-Ion batteries. *J. Electrochem. Soc.* 160, A569–A574. doi: 10.1149/2.032304jes
- Mu, L., Xu, S., Li, Y., Hu, Y.-S., Li, H., Chen, L., et al. (2015). Prototype sodium-ion batteries using an air-stable and Co/Ni-Free O3-layered metal oxide cathode. *Adv. Mater.* 27, 6928–6933. doi: 10.1002/adma.201502449
- Nayak, P. K., Yang, L., Brehm, W., and Adelhelm, P. (2018). From lithium-ion to sodium-ion batteries: advantages, challenges, and surprises. *Angew. Chem. Int. Ed.* 57, 102–120. doi: 10.1002/anie.201703772
- Ono, Y. (2018). Structural analysis of  $NaCuO_2$  cathode at various charged/discharged stages and its reaction mechanism. *Electrochemistry* 86, 309–314. doi: 10.5796/electrochemistry.18-6-E2674
- Ono, Y., Yui, Y., Hayashi, M., Asakura, K., Kitabayashi, H., and Takahashi, K. I. (2014). Electrochemical properties of  $NaCuO_2$  for sodium-ion secondary batteries. *ECS Trans.* 58, 33–39. doi: 10.1149/05812.0033ecst
- Palomares, V., Casas-Cabanas, M., Castillo-Martinez, E., Han, M. H., and Rojo, T. (2013). Update on Na-based battery materials. A growing research path. *Energy Environ. Sci.* 6, 2312–2337. doi: 10.1039/c3ee41031e
- Pan, H., Hu, Y.-S., and Chen, L. (2013). Room-temperature stationary sodium-ion batteries for large-scale electric energy storage. *Energy Environ. Sci.* 6, 2338–2360. doi: 10.1039/c3ee40847g
- Paulsen, J. M., and Dahn, J. R. (1999). Studies of the layered manganese bronzes,  $Na_{2/3}[Mn_{1-x}M_x]O_2$  with  $M=Co, Ni, Li$ , and  $Li_{2/3}[Mn_{1-x}M_x]O_2$  prepared by ion-exchange. *Solid State Ionics* 126, 3–24. doi: 10.1016/S0167-2738(99)00147-2
- Qi, X., Wang, Y., Jiang, L., Mu, L., Zhao, C., Liu, L., et al. (2016). Sodium-Deficient O3- $Na_{0.9}Ni_{0.4}Mn_xTi_{0.6-x}O_2$  Layered-Oxide Cathode Materials for Sodium-Ion Batteries. *Part. Part. Syst. Charact.* 33, 538–544. doi: 10.1002/ppsc.201500129
- Qian, J., Wu, C., Cao, Y., Ma, Z., Huang, Y., Ai, X., et al. (2018). Sodium-ion batteries: prussian blue cathode materials for sodium-ion batteries and other ion batteries. *Adv. Energy Mater.* 8:1870079. doi: 10.1002/aenm.201870079
- Qiao, Y., Guo, S., Zhu, K., Liu, P., Li, X., Jiang, K., et al. (2018). Reversible anionic redox activity in  $Na_3RuO_4$  cathodes: a prototype Na-rich layered oxide. *Energy Environ. Sci.* 11, 299–305. doi: 10.1039/C7EE03554C
- Rai, A. K., Anh, L. T., Gim, J., Mathew, V., and Kim, J. (2014). Electrochemical properties of  $Na_xCoO_2$  ( $x \sim 0.71$ ) cathode for rechargeable sodium-ion batteries. *Ceram. Int.* 40, 2411–2417. doi: 10.1016/j.ceramint.2013.08.013
- Roger, M., Morris, D. J., Tennant, D. A., Gutmann, M. J., Goff, J. P., Hoffmann, J.-U., et al. (2007). Patterning of sodium ions and the control of electrons in sodium cobaltate. *Nature* 445:631. doi: 10.1038/nature05531
- Rong, X., Liu, J., Hu, E., Liu, Y., Wang, Y., Wu, J., et al. (2018). Structure-induced reversible anionic redox activity in Na layered oxide cathode. *Joule* 2, 125–140. doi: 10.1016/j.joule.2017.10.008
- Rozier, P., Sathiy, M., Paulraj, A.-R., Foix, D., Desaunay, T., Taberna, P.-L., et al. (2015). Anionic redox chemistry in Na-rich  $Na_2Ru_{1-y}Sn_yO_3$  positive electrode material for Na-ion batteries. *Electrochem. Commun.* 53, 29–32. doi: 10.1016/j.elecom.2015.02.001
- Saadoune, I., Maazaz, A., Ménétrier, M., and Delmas, C. (1996). On the  $Na_xNi_{0.6}Co_{0.4}O_2$  system: physical and electrochemical studies. *J. Solid State Chem.* 122, 111–117. doi: 10.1006/jssc.1996.0090
- Sabi, N., Doubaji, S., Hashimoto, K., Komaba, S., Amine, K., Solhy, A., et al. (2017). Layered P2- $Na_{2/3}Co_{1/2}Ti_{1/2}O_2$  as a high-performance cathode material for sodium ion batteries. *J. Power Sources* 342, 998–1005. doi: 10.1016/j.jpowsour.2017.01.025
- Sathiy, M., Hemalatha, K., Ramesha, K., Tarascon, J. M., and Prakash, A. S. (2012). Synthesis, structure, and electrochemical properties of the layered sodium insertion cathode material:  $NaNi_{1/3}Mn_{1/3}Co_{1/3}O_2$ . *Chem. Mater.* 24, 1846–1853. doi: 10.1021/cm300466b
- Sathiy, M., Jaquet, Q., Doublet, M.-L., Karakulina, O. M., Hadermann, J., and Tarascon, J.-M. (2018). A chemical approach to raise cell voltage and suppress phase transition in O3 sodium layered oxide electrodes. *Adv. Energy Mater.* 0, 1702599. doi: 10.1002/aenm.201702599
- Satyanarayana, M., Jibin, A. K., and Varadaraju, U. V. (2016). Synthesis, structural and electrochemical study of O3- $NaNi_{0.4}Mn_{0.4}Co_{0.2}O_2$  as a cathode material for Na-ion batteries. *Rsc Adv.* 6, 61334–61340. doi: 10.1039/C6RA06785A
- Senguttuvan, P., Rousse, G., Seznec, V., Tarascon, J.-M., and Palacin, M. R. (2011).  $Na_2Ti_3O_7$ : lowest voltage ever reported oxide insertion electrode for sodium ion batteries. *Chem. Mater.* 23, 4109–4111. doi: 10.1021/cm202076g
- Shannon, R. D. (1976). Revised effective ionic-radii and systematic studies of interatomic distances in halides and chalcogenides. *Acta Crystallogr. Sect. A* 32, 751–767. doi: 10.1107/S0567739476001551
- Shu, G. J., and Chou, F. C. (2008). Sodium-ion diffusion and ordering in single-crystal P2- $Na_xCoO_2$ . *Phys. Rev. B* 78:052101. doi: 10.1103/PhysRevB.78.052101
- Song, S., Kotobuki, M., Chen, Y., Manzhos, S., Xu, C., Hu, N., et al. (2017). Na-rich layered  $Na_2Ti_{1-x}Cr_xO_{3-x/2}$  ( $x = 0, 0.06$ ): Na-ion battery cathode materials with high capacity and long cycle life. *Sci. Rep.* 7:373. doi: 10.1038/s41598-017-00346-x
- Su, D., Cortie, M., Fan, H., and Wang, G. (2017). Prussian blue nanocubes with an open framework structure coated with PEDOT as high-capacity cathodes for lithium-sulfur batteries. *Adv. Mater.* 29:1700587. doi: 10.1002/adma.201700587
- Sun, X., Ji, X.-Y., Xu, H.-Y., Zhang, C.-Y., Shao, Y., Zang, Y., et al. (2016). Sodium insertion cathode material  $Na_{0.67}Ni_{0.4}Co_{0.2}Mn_{0.4}O_2$  with excellent electrochemical properties. *Electrochim. Acta* 208, 142–147. doi: 10.1016/j.electacta.2016.04.067
- Thackeray, M. M., Shao-Horn, Y., Kahaian, A. J., Kepler, K. D., Skinner, E., Vaughey, J. T., et al. (1998). Structural fatigue in spinel electrodes in high voltage (4V)  $Li/Li_xMn_2O_4$  cells. *Electrochem. Solid-State Lett.* 1, 7–9. doi: 10.1149/1.1390617
- Toumar, A. J., Ong, S. P., Richards, W. D., Dacek, S., and Cedert G. (2015). Vacancy ordering in O3-type layered metal oxide sodium-ion battery cathodes. *Phys. Rev. Appl.* 4:064002. doi: 10.1103/PhysRevApplied.4.064002
- Tripathi, R., Wood, S. M., Islam, M. S., Nazar, L., and Nazar, L. F. (2013). Na-ion mobility in layered  $Na_2FePO_4F$  and organic  $Na[Fe,Mn]PO_4$ . *Energy Environ. Sci.* 6, 2257–2264. doi: 10.1039/c3ee40914g
- Vassilaras, P., Ma, X., Li, X., and Ceder, G. (2013). Electrochemical properties of monoclinic  $NaNiO_2$ . *J. Electrochem. Soc.* 160, A207–A211. doi: 10.1149/2.023302jes
- Vassilaras, P., Toumar, A. J., and Ceder, G. (2014). Electrochemical properties of  $NaNi_{1/3}Co_{1/3}Fe_{1/3}O_2$  as a cathode material for Na-ion batteries. *Electrochem. Commun.* 38, 79–81. doi: 10.1016/j.elecom.2013.11.015
- Wang, H., Gu, M., Jiang, J., Lai, C., and Ai, X. (2016a). An O3-type  $NaNi_{0.5}Mn_{0.3}Ti_{0.2}O_2$  compound as new cathode material for room-temperature sodium-ion batteries. *J. Power Sources* 327, 653–657. doi: 10.1016/j.jpowsour.2016.07.109

- Wang, J., He, X., Zhou, D., Schappacher, F., Zhang, X., Liu, H., et al. (2016b). O3-type Na[Fe<sub>1/3</sub>Ni<sub>1/3</sub>Ti<sub>1/3</sub>]O<sub>2</sub> cathode material for rechargeable sodium ion batteries. *J. Mater. Chem. A* 4, 3431–3437. doi: 10.1039/C5TA10520J
- Wang, L., Sun, Y.-G., Hu, L.-L., Piao, J.-Y., Guo, J., Manthiram, A., et al. (2017). Copper-substituted Na<sub>0.67</sub>Ni<sub>0.3-x</sub>Cu<sub>x</sub>Mn<sub>0.7</sub>O<sub>2</sub> cathode materials for sodium-ion batteries with suppressed P2-O2 phase transition. *J. Mater. Chem. A* 5, 8752–8761. doi: 10.1039/C7TA00880E
- Wang, P.-F., Xin, H., Zuo, T.-T., Li, Q., Yang, X., Yin, Y.-X., et al. (2018b). An abnormal 3.7 Volt O3-type sodium-ion battery cathode. *Angew. Chem. Int. Ed.* 57, 8178–8183. doi: 10.1002/anie.201804130
- Wang, P.-F., Yao, H.-R., Liu, X.-Y., Zhang, J.-N., Gu, L., Yu, X.-Q., et al. (2017). Ti-substituted NaNi<sub>0.5</sub>Mn<sub>0.5-x</sub>Ti<sub>x</sub>O<sub>2</sub> cathodes with reversible O3–P3 phase transition for high-performance sodium-ion batteries. *Adv. Mater.* 29:1700210. doi: 10.1002/adma.201700210
- Wang, P.-F., You, Y., Yin, Y.-X., and Guo, Y.-G. (2016d). An O3-type NaNi<sub>0.5</sub>Mn<sub>0.5</sub>O<sub>2</sub> cathode for sodium-ion batteries with improved rate performance and cycling stability. *J. Mater. Chem. A* 4, 17660–17664. doi: 10.1039/C6TA07589D
- Wang, P.-F., You, Y., Yin, Y.-X., and Guo, Y.-G. (2018c). Layered oxide cathodes for sodium-ion batteries: phase transition, air stability, and performance. *Adv. Energy Mater.* 8:1701912. doi: 10.1002/aenm.201701912
- Wang, P.-F., You, Y., Yin, Y.-X., Wang, Y.-S., Wan, L.-J., Gu, L., et al. (2016c). Suppressing the P2–O2 phase transition of Na<sub>0.67</sub>Mn<sub>0.67</sub>Ni<sub>0.33</sub>O<sub>2</sub> by magnesium substitution for improved sodium-ion batteries. *Angew. Chem. Int. Ed. Engl.* 55, 7445–7449. doi: 10.1002/anie.201602202
- Wang, P. F., Yao, H. R., Liu, X. Y., Yin, Y.-X., Zhang, J. N., Wen, Y., et al. (2018a). Na<sup>(+)</sup>/vacancy disordering promises high-rate Na-ion batteries. *Sci. Adv.* 4:eaar6018. doi: 10.1126/sciadv.aar6018
- Wang, Q., Xu, J., Zhang, W., Mao, M., Wei, Z., Wang, L., et al. (2018d). Research progress on vanadium-based cathode materials for sodium ion batteries. *J. Mater. Chem. A* 6, 8815–8838. doi: 10.1039/C8TA01627E
- Wang, Y., Xiao, R., Hu, Y. S., Avdeev, M., and Chen, L. (2015). P2-Na<sub>0.6</sub>[Cr<sub>0.6</sub>Ti<sub>0.4</sub>]O<sub>2</sub> cation-disordered electrode for high-rate symmetric rechargeable sodium-ion batteries. *Nat. Commun.* 6:6954. doi: 10.1038/ncomms7954
- Wu, D., Li, X., Xu, B., Twu, N., Liu, L., and Ceder, G. (2015). NaTiO<sub>2</sub>: a layered anode material for sodium-ion batteries. *Energy Environ. Sci.* 8, 195–202. doi: 10.1039/C4EE03045A
- Wu, X., Guo, J., Wang, D., Zhong, G., McDonald, M. J., and Yang, Y. (2015). P2-type Na<sub>0.66</sub>Ni<sub>0.33-x</sub>Zn<sub>x</sub>Mn<sub>0.67</sub>O<sub>2</sub> as new high-voltage cathode materials for sodium-ion batteries. *J. Power Sources* 281, 18–26. doi: 10.1016/j.jpowsour.2014.12.083
- Xiang, X., Zhang, K., and Chen, J. (2015). Recent advances and prospects of cathode materials for sodium-ion batteries. *Adv. Mater.* 27, 5343–5364. doi: 10.1002/adma.201501527
- Xu, J., Lee, D. H., Clément, R. J., Yu, X., Leskes, M., Pell, A. J., et al. (2014). Identifying the critical role of Li substitution in P2-Na<sub>x</sub>[Li<sub>y</sub>Ni<sub>z</sub>Mn<sub>1-y-z</sub>]O<sub>2</sub> (0 < x, y, z < 1) intercalation cathode materials for high-energy Na-Ion batteries. *Chem. Mater.* 26, 1260–1269. doi: 10.1021/cm403855t
- Yabuuchi, N., Kajiyama, M., Iwatate, J., Nishikawa, H., Hitomi, S., Okuyama, R., et al. (2012a). P2-type Na<sub>x</sub>[Fe<sub>1/2</sub>Mn<sub>1/2</sub>]O<sub>2</sub> made from earth-abundant elements for rechargeable Na batteries. *Nat. Mater.* 11, 512–517. doi: 10.1038/nmat3309
- Yabuuchi, N., Kubota, K., Dahbi, M., and Komaba, S. (2014). Research development on sodium-ion batteries. *Chem. Rev.* 114, 11636–11682. doi: 10.1021/cr500192f
- Yabuuchi, N., Yoshida, H., and Komaba, S. (2012b). Crystal structures and electrode performance of alpha-NaFeO<sub>2</sub> for rechargeable sodium batteries. *Electrochemistry* 80, 716–719. doi: 10.5796/electrochemistry.80.716
- Yang, J., Wang, Y., Li, W., Wang, L., Fan, Y., Jiang, W., et al. (2017). Amorphous TiO<sub>2</sub> shells: a vital elastic buffering layer on silicon nanoparticles for high-performance and safe lithium storage. *Adv. Mater.* 29:1700523. doi: 10.1002/adma.201700523
- Yang, Z., Zhang, J., Kintner-Meyer, M. C., Lu, X., Choi, D., Lemmon, J. P., et al. (2011). Electrochemical energy storage for green grid. *Chem. Rev.* 111, 3577–3613. doi: 10.1021/cr100290v
- Yao, H.-R., Wang, P.-F., Gong, Y., Zhang, J., Yu, X., Gu, L., et al. (2017). Designing air-stable O3-type cathode materials by combined structure modulation for Na-Ion batteries. *J. Am. Chem. Soc.* 139, 8440–8443. doi: 10.1021/ja.cs.7b05176
- You, Y., Dolocan, A., Li, W., and Manthiram, A. (2018). Understanding the air-exposure degradation chemistry at a nanoscale of layered oxide cathodes for sodium-ion batteries. *Nano Lett.* 19, 182–188. doi: 10.1021/acs.nanolett.8b03637
- You, Y., Kim, S. O., and Manthiram, A. (2017). A Honeycomb-layered oxide cathode for sodium-ion batteries with suppressed P3–O1 phase transition. *Adv. Energy Mater.* 7:1601698. doi: 10.1002/aenm.201601698
- Yu, C.-Y., Park, J.-S., Jung, H.-G., Chung, K.-Y., Aurbach, D., Sun, Y.-K., et al. (2015). NaCrO<sub>2</sub> cathode for high-rate sodium-ion batteries. *Energy Environ. Sci.* 8, 2019–2026. doi: 10.1039/C5EE00695C
- Yue, J.-L., Yin, W.-W., Cao, M.-H., Zulipiya, S., Zhou, Y.-N., and Fu, Z.-W. (2015). A quinary layer transition metal oxide of NaNi<sub>1/4</sub>Co<sub>1/4</sub>Fe<sub>1/4</sub>Mn<sub>1/8</sub>Ti<sub>1/8</sub>O<sub>2</sub> as a high-rate-capability and long-cycle-life cathode material for rechargeable sodium ion batteries. *Chem. Commun.* 51, 15712–15715. doi: 10.1039/C5CC06585B
- Zhang, X.-H., Pang, W.-L., Wan, F., Guo, J.-Z., Lu, H.-Y., Li, J.-Y., et al. (2016). P2-Na<sub>2/3</sub>Ni<sub>1/3</sub>Mn<sub>5/9</sub>Al<sub>1/9</sub>O<sub>2</sub> microparticles as superior cathode material for sodium-ion batteries: enhanced properties and mechanism via graphene connection. *ACS Appl. Mater. Interfaces* 8, 20650–20659. doi: 10.1021/acsami.6b03944
- Zhang, Y., Zhao, H., and Du, Y. (2016). Symmetric full cells assembled by using self-supporting Na<sub>3</sub>V<sub>2</sub>(PO<sub>4</sub>)<sub>3</sub> bipolar electrodes for superior sodium energy storage. *J. Mater. Chem. A* 4, 7155–7159. doi: 10.1039/C6TA02218A
- Zheng, C., Radhakrishnan, B., Chu, I.-H., Wang, Z., and Ong, S. P. (2017). Effects of transition-metal mixing on Na ordering and kinetics in layered P2 oxides. *Phys. Rev. Appl.* 7:064003. doi: 10.1103/PhysRevApplied.7.064003
- Zheng, L., Li, J., and Obrovac, M. N. (2017). Crystal structures and electrochemical performance of air-stable Na<sub>2/3</sub>Ni<sub>1/3-x</sub>Cu<sub>x</sub>Mn<sub>2/3</sub>O<sub>2</sub> in sodium cells. *Chem. Mater.* 29, 1623–1631. doi: 10.1021/acs.chemmater.6b04769
- Zheng, L., and Obrovac, M. N. (2017). Investigation of O3-type Na<sub>0.9</sub>Ni<sub>0.45</sub>Mn<sub>x</sub>Ti<sub>0.55-x</sub>O<sub>2</sub> (0 ≤ x ≤ 0.55) as positive electrode materials for sodium-ion batteries. *Electrochim. Acta* 233, 284–291. doi: 10.1016/j.electacta.2017.03.033
- Zhu, G., Zhang, F., Li, X., Luo, W., Li, L., Zhang, H., et al. (2019). Engineering the distribution of carbon in silicon oxide nanospheres at atomic level for highly stable anodes. *Angew Chem Int Ed Engl* 58, 1–6. doi: 10.1002/anie.2019.02083
- Zhu, H., Lee, K. T., Hitz, G. T., Han, X., Li, Y., Wan, J., et al. (2014). Free-standing Na<sub>2/3</sub>Fe<sub>1/2</sub>Mn<sub>1/2</sub>O<sub>2</sub>@graphene film for a sodium-ion battery cathode. *ACS Appl. Mater. Interfaces* 6, 4242–4247. doi: 10.1021/am405970s
- Zhu, Y.-E., Qi, X., Chen, X., Zhou, X., Zhang, X., Wei, J., et al. (2016). A P2-Na<sub>0.67</sub>Co<sub>0.5</sub>Mn<sub>0.5</sub>O<sub>2</sub> cathode material with excellent rate capability and cycling stability for sodium ion batteries. *J. Mater. Chem. A* 4, 11103–11109. doi: 10.1039/C6TA02845D

**Conflict of Interest Statement:** The authors declare that the research was conducted in the absence of any commercial or financial relationships that could be construed as a potential conflict of interest.

Copyright © 2019 Zhang, Zhang and Huang. This is an open-access article distributed under the terms of the Creative Commons Attribution License (CC BY). The use, distribution or reproduction in other forums is permitted, provided the original author(s) and the copyright owner(s) are credited and that the original publication in this journal is cited, in accordance with accepted academic practice. No use, distribution or reproduction is permitted which does not comply with these terms.